





Subduction-related Late Cretaceous high-K volcanism in the Central Pontides orogenic belt: constraints on geodynamic implications

Emre Aydınçakır


To cite this article: Emre Aydınçakır (2016) Subduction-related Late Cretaceous high-K volcanism in the Central Pontides orogenic belt: constraints on geodynamic implications, *Geodinamica Acta*, 28:4, 379-411, DOI: [10.1080/09853111.2016.1208526](https://doi.org/10.1080/09853111.2016.1208526)

To link to this article: <http://dx.doi.org/10.1080/09853111.2016.1208526>

 View supplementary material [↗](#)

 Published online: 18 Jul 2016.

 Submit your article to this journal [↗](#)

 Article views: 75

 View related articles [↗](#)

 View Crossmark data [↗](#)

Subduction-related Late Cretaceous high-K volcanism in the Central Pontides orogenic belt: constraints on geodynamic implications

Emre Aydınçakır*

Department of Geological Engineering, Gümüşhane University, Gümüşhane TR-29000, Turkey

(Received 5 January 2016; accepted 29 June 2016)

Mineral chemistry, major and trace elements, $^{40}\text{Ar}/^{39}\text{Ar}$ age and Sr–Nd–Pb isotopic data are presented for the Late Cretaceous Hamsilos volcanic rocks in the Central Pontides, Turkey. The Hamsilos volcanic rocks mainly consist of basalt, andesite and associated pyroclastics (volcanic breccia, vitric tuff and crystal tuff). They display shoshonitic and high-K calc-alkaline affinities. The shoshonitic rocks contain plagioclase, clinopyroxene, alkali feldspar, phlogopite, analcime, sanidine, olivine, apatite and titanomagnetite, whereas the high-K calc-alkaline rocks contain plagioclase, clinopyroxene, orthopyroxene, magnetite / titanomagnetite in microgranular porphyritic, hyalo-microlitic porphyritic and glomeroporphyritic matrix. Mineral chemistry data reveal that the pressure condition of the clinopyroxene crystallisation for the shoshonitic rocks are between 1.4 and 6.3 kbar corresponds to 6–18-km depth and the high-K calc-alkaline rocks are between 5 and 12 km. $^{40}\text{Ar}/^{39}\text{Ar}$ age data changing between $72 \pm .5$ Ma and $79.0 \pm .3$ Ma (Campanian) were determined for the Late Cretaceous Hamsilos volcanic rocks, contemporaneous with the subduction of the Neo-Tethyan Ocean beneath the Pontides. The studied volcanic rocks were enriched in the large-ion lithophile and light rare earth element contents, with pronounced depletion in the contents of high-field-strength elements. Chondrite-normalised rare earth element patterns ($\text{La}_N/\text{Lu}_N = 6\text{--}17$) show low to medium enrichment, indicating similar sources of the rock suite. Initial $^{87}\text{Sr}/^{86}\text{Sr}$ values vary between .70615 and .70796, whereas initial $^{143}\text{Nd}/^{144}\text{Nd}$ values change between .51228 and .51249. Initial $^{206}\text{Pb}/^{204}\text{Pb}$ values vary between 18.001 and 18.349, $^{207}\text{Pb}/^{204}\text{Pb}$ values between 15.611 and 15.629 and $^{208}\text{Pb}/^{204}\text{Pb}$ values between 37.839 and 38.427. The main solidification processes involved in the evolution of the volcanic rocks consist of fractional crystallisation, with minor amounts of crustal contamination \pm magma mixing. According to geochemical evidence, the shoshonitic melts in the Hamsilos volcanic rocks were possibly derived from the low degree of partial melting of a subcontinental lithospheric mantle (SCLM), while the high-K calc-alkaline melts were derived from relatively high degree of partial melting of SCLM that was enriched by fluids and/or sediments from a subduction of oceanic crust.

Keywords: $^{40}\text{Ar}/^{39}\text{Ar}$ ages; Sr–Nd–Pb isotopes; Hamsilos; subduction; Turkey

1. Introduction

The Pontides orogenic belt, a prominent part of the Alpine–Himalayan Orogen, is a typical place to understand the nature of subduction-related magmatism. Previous studies provided certain geochronological and geochemical constraints on the origin and evolution of Late Cretaceous magmatism. The geochemical nature of the great majority of Late Cretaceous magmatism is of calc-alkaline (Aydın, 2014; Ercan & Gedik, 1983; Karsli et al., 2010; Kaygusuz & Aydınçakır, 2009, 2011; Tokel, 1983). However, rare volcanic and plutonic bodies, such as those in this study, attained high-K to shoshonitic composition (Altherr et al., 2008; Asan, Kurt, Francis, & Morgan, 2014; Bektas & Gedik, 1988; Eyüboğlu, 2010; Genç et al., 2014; Gülmez & Genc, 2015; Karsli et al., 2012; Varol, 2013). According to a widely accepted tectonic model (Aydınçakır, 2014; Dokuz et al., 2013; Karsli, Uysal, Dilek, Aydın, & Kandemir, 2013; Okay & Şahintürk, 1997; Okay & Tüysüz, 1999; Şengör & Yılmaz, 1981; Ustaomer & Robertson, 2010), the Late Cretaceous magmatism is associated with the northward subduction of the northern branch of the Neotethys

Ocean beneath the southern margin of the Eurasian Plate during the late Cretaceous to Paleocene (Figure 1(a)). The subduction polarity and geotectonic evolution of the eastern Pontides are controversial during the Cretaceous. Several researchers suggested that the eastern Pontides was a magmatic arc that occurred as a result of northward subduction of the Neotethys along the southern border of the Sakarya Zone (Altherr et al., 2008; Karsli et al., 2010; Okay & Şahintürk, 1997; Şengör, Özeren, Genç, & Zor, 2003; Ustaomer & Robertson, 2010). Conversely, Dewey, Pıtman, Ryan, and Bonnin (1973), Bektaş, Şen, Atici, and Köprübaşı (1999), Eyuboglu, Chung, Santosh, Dudas, and Akaryalı (2011), and Eyuboglu, Santosh, Dudas, Chung, and Akaryalı (2011) proposed a southward subduction that continued uninterruptedly from the Paleozoic period until the end of the Eocene period.

The petrogenesis and tectonic setting of high-K to shoshonitic volcanic rocks from the Eastern Pontides remain controversial (Altherr et al., 2008; Asan et al., 2014; Bektas & Gedik, 1988; Eyüboğlu, 2010; Genç et al., 2014; Gülmez & Genc, 2015). Genç et al. (2014)

*Email: emre@gumushane.edu.tr, aydincakir61@gmail.com

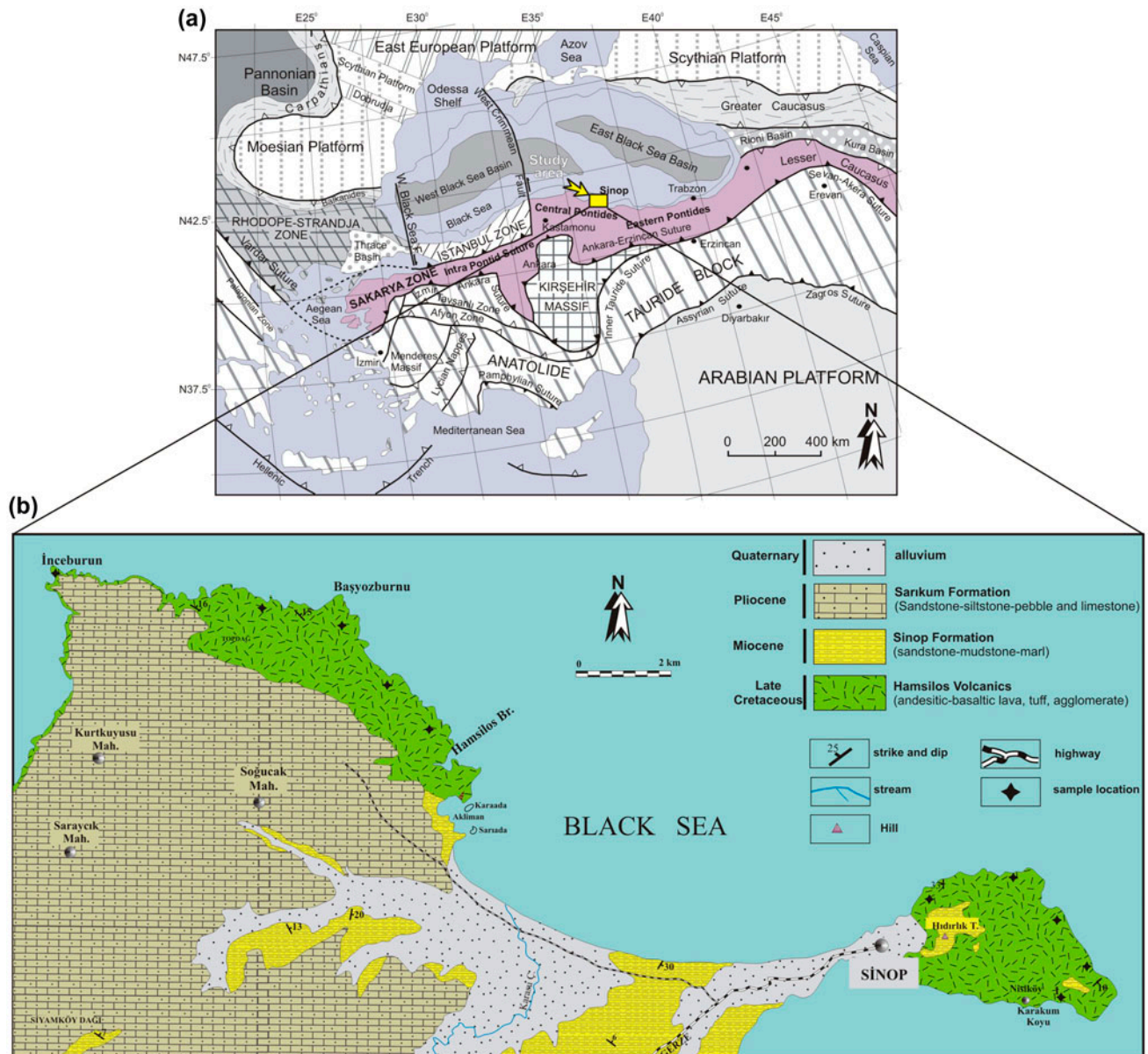


Figure 1. (a) Regional tectonic setting of Turkey with main tectonic units in relation to the Afro-Arabian and Eurasian plates (modified from Okay & Tüysüz, 1999). (b) Simplified geological map of the Sinop area showing the Late Cretaceous Hamsilos volcanic rocks with sample locations (modified after Baş, 1986; Gedik & Korkmaz, 1984).

offered that ultrapotassic rocks were possibly derived from the low degree partial melting of veined subcontinental lithospheric mantle (SCLM) that occurred as a result of northward subduction of the Neotethys. Alther et al. (2008) proposed that ultrapotassic rocks and their orogenic nature indicate that during the last stages of the closure of the northern branch of Neotethys. Conversely, Eyüboğlu (2010) suggested that these rocks were derived from enriched mantle sources that are related to southward subduction of the Neotethys.

Such high-K composition of rocks can be produced from crust and mantle rocks through various petrogenetic processes, such as (i) partial melting of basaltic rocks at the lower crust (Sisson, Ratajeski, Hankins, & Glazner, 2005), (ii) fractional crystallisation and crustal contami-

nation (assimilation-fractional crystallisation [AFC]) of mantle-derived basaltic magmas (Chen, Hegner, & Todt, 2000) and (iii) mixing of mantle and crustal magmas (Griffin et al., 2002) in various tectonic settings, such as volcanic island arc, active continental margin and post-collision (Barbarin, 2005).

However, there has been much less work on the classification and geochemistry of the Upper Cretaceous high-K volcanic rocks exposed in the central and southern part of the Pontides. Bektas and Gedik (1988) first recognised leucite-bearing volcanic rocks (Everekhanları Formation, Bayburt) in southern part of the eastern Pontides. Eyüboğlu (2010) suggested that trachyan-desites- and analcime-bearing volcanics were derived from similar enriched mantle sources, and that they

formed in the same geotectonic setting of a back-arc basin environment of the eastern Pontide magmatic arc during the Late Cretaceous. Similar shoshonitic and ultrapotassic volcanism are reported from Gümüşhacıköy near Amasya and Ankara (Çapan, 1984; Eyüboğlu, 2010; Varol, 2013). Apart from these locations, there are also Hamsilos volcanics containing analcime-bearing rocks around Sinop to the north (e.g. Baş, 1986). Asan et al. (2014) stated that Hamsilos volcanics display high-K calc-alkaline, shoshonitic and ultra-K affinities. Otherwise, the shoshonitic and ultra-K were derived from metasomatic veins related to melting of recycled subducted sediments, but the high-K calc-alkaline rocks from a lithospheric source metasomatised by fluids from subduction zone.

Unlike previous studies, volcanic stratigraphy determination, textural petrography and mineral chemistry studies on these volcanics are often ruled out in paper (Asan et al., 2014) evaluating magmatic crystallisation conditions and magma chamber processes. In the present paper, (1) mineral chemistry data in order to determine physicochemical conditions in terms of intensive parameters (P and T) are presented to define emplacement and crystallisation conditions of the magma(s); (2) furnish a general evolutionary model for magma chamber processes on the basis of composition of mid-, and shallow-continental crusts; (3) the origin of analcime (primary or secondary), (4) geochronological, geochemical and isotopic data are presented to examine the petrogenesis and tectonic implications of the Hamsilos volcanic rocks from the Sakarya Zone, as well as to constrain the involved geodynamic processes.

2. Regional geology and geological setting

The northern part of Turkey comprises three main tectonic zones, namely Istranca, Istanbul and Sakarya, which are collectively known as Pontides (Figure 1(a); Şengör & Yılmaz, 1981; Okay & Tüysüz, 1999). The Pontides belt, which extends between the Lesser Caucasus in the east and the Balkans in the west, is divided into three regions because of the different tectonic units they include: ‘western Pontides’, ‘Central Pontides’ and ‘eastern Pontides’. The Sakarya Zone, which extends from the Biga Peninsula to eastern Pontides and performs an important function in plate tectonics, is an Alpine tectonic assembly located between the Intra-Pontide in the north and Izmir–Ankara–Erzincan suture zones in the south (Okay, 2011).

The ‘Central Pontides’ is a geographical term comprising the middle portions of the Sakarya Zone (Okay et al., 2006). This region, which includes the study area, is a place where an important continental growth occurred on the continental margin of Laurasia because of the subduction of the Tethys Ocean during the Mesozoic (Aygül & Okay, 2012). The Central Pontides is bordered by the Black Sea in the north and separated from the Izmir–Ankara–Erzincan suture zone and Central

Anatolian Crystalline Complex in the south. The Central Pontides comprising of İstanbul and Sakarya Zones encountered during the Eocene and younger units lie in the north; it also contains Black Sea marginal basin deposits (Cretaceous–Eocene volcano-sedimentary sequences) bordered by the Black Sea in the farther north (Okay et al., 2006; Tüysüz, 1990; Ustaömer & Robertson, 1993; Yılmaz & Şengör, 1985; Figure 1(b)). These zones started to exist alongside each other together with the tectonic opening of the Black Sea basin in the Early Cretaceous Period (Tüysüz, 1999) and were formed by the tectonic mixing of the Cimmerian and Eurasian continental remnants with Paleotethys Ocean remnants (Yılmaz, Tüysüz, Yiğitbaş, Genç, & Şengör, 1997). The İstanbul Zone is dominated by passive margin type Ordovician–Carboniferous-sedimentary successions, which were unconformably covered by Triassic and younger units (Görür, et al. 1997). On the contrary, the Sakarya Zone was formed by Permo–Triassic subduction–accretion complexes and unconformably covered by Triassic and younger sediments (Genç & Yılmaz, 1995; Goncuoglu, Turhan, & Tekin, 2003; Okay & Tüysüz, 1999; Tekeli, 1981).

Hamsilos volcanic, main topic of this study, cover a large area in the Sinop Peninsula (the shoshonitic rocks), and Inceburun Peninsula (high-K calc-alkaline rocks) (Asan et al., 2014; Aydınçakır & Şen, 2011; Baş, 1986). There is no physical contact and systematic change between high-K calc-alkaline and shoshonitic rocks.

These volcanic mainly consist of basaltic lava flows, basalt dikes, brecciated volcanoclastics, agglomerates and tuffs (Figure 2). Basalt dikes and lavas are dominant in Inceburun Peninsula (Figure 2(a) and (b)). Fresh surfaces are characteristically dark and grey coloured basalt lavas (Figure 2(a) and (b)). Agglomerates, brecciated volcanoclastics and tuffs prevail on the Sinop Peninsula (Figure 2(c) and (d)). Tuffs are minor constituents of the sequence. Breccias are characterised by reddish and grey colour with fragments 5–35 cm in diameter and varying angular to rounded shape (Figure 2(c)). Euhedral to subhedral pyroxene and mica minerals are easily seen in basaltic lavas (Figure 2(d)). Cavities in the basaltic lavas have been generally filled by secondary calcite and zeolites.

Hamsilos volcanites are covered by Sinop Formation, which is formed from the sandstone, claystone and marl alternation of the Miocene period. The Sarıkum Formation and the alluvium are the younger sedimentary successions of the region.

3. Analytical methods

3.1 Whole-rock geochemical analyses

Based on the petrographical studies, 20 of the freshest and most representative rock samples from the volcanics were selected for major and trace element analyses (Table 5). To prepare the rock powders, .5–1 kg of the fresh samples was crushed in a steel jaw crusher, and then the samples were powdered in an agate mill to

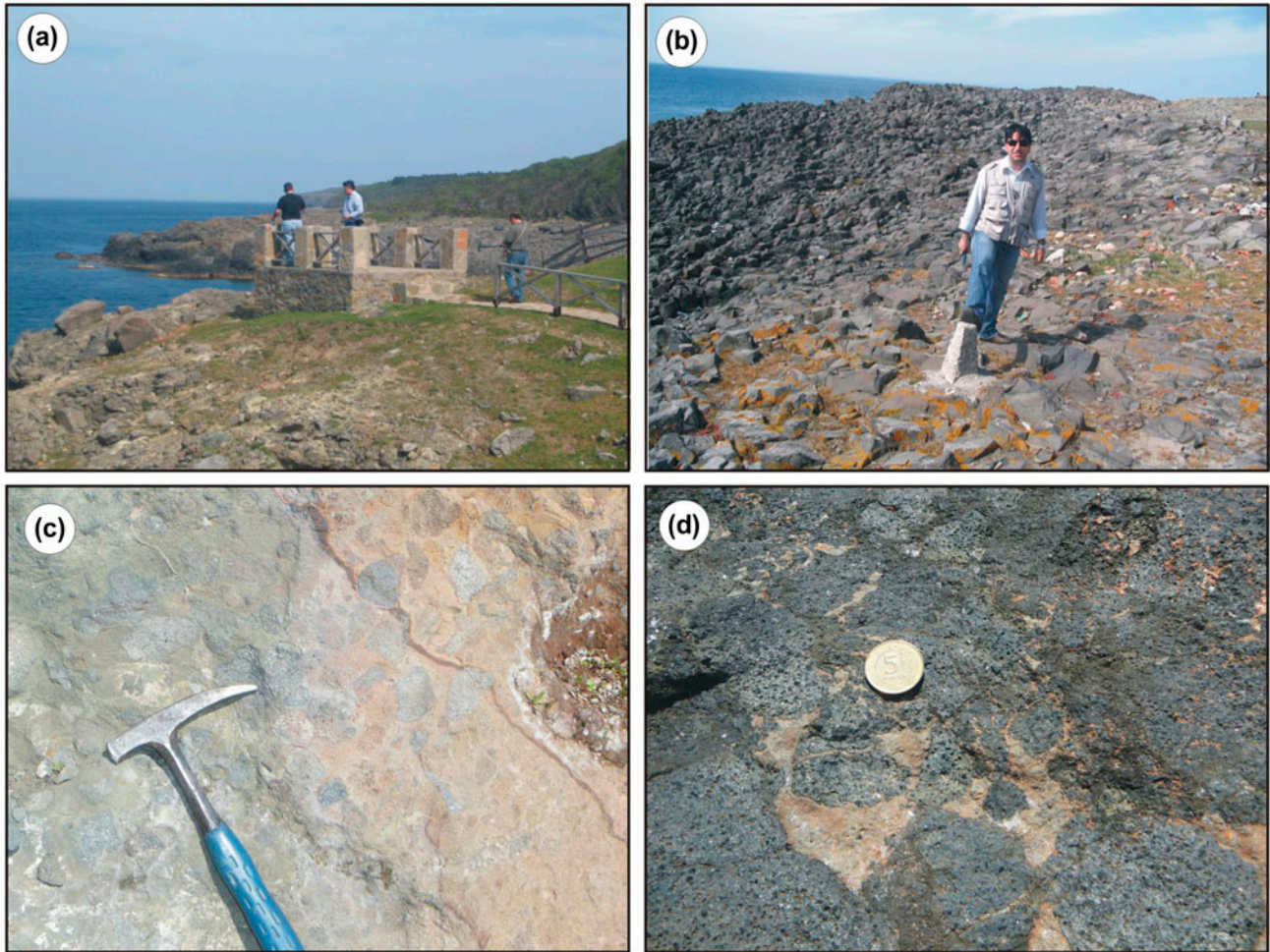


Figure 2. Field views of (a, b) the basalt lavas are dominant in the high-K calc-alkaline around Inceburun Peninsula, (c, d) the agglomerates, brecciated volcaniclastics and tuffs in the Sinop Peninsula.

obtain grain sizes of <200 mesh. The major and trace element compositions were measured by ICP-AES at the commercial ACME Analytical Laboratories Ltd, in Vancouver, Canada after .2 g samples of rock powder were fused with 1.5 g LiBO_2 and then dissolved via four-acid digestion steps. The loss on ignition (LOI) was determined by the weight difference after ignition at 1000 °C. The total iron concentration was expressed as Fe_2O_3 . The detection limits are in the range of .001–.1 wt% for major element oxides, .1–10 ppm for trace elements and .01–.5 ppm for rare earth element (REE). Calibration and verification standards together with reagent blanks were added to the sample sequence. STD SO 18 was certified in-house against 38 certified reference material including CANMET SY-4 and USGS AGV-1, G-2, GSP-2 and W-2 as known external standards. The analytical accuracy is better than 4%.

3.2 Microchemical analyses

Electron microprobe analyses on polished thin sections were carried out at the New Mexico Institute of Mining and Technology, Socorro, NM, USA, using a Cameca

SX-100 electron microprobe with three wavelength-dispersive spectrometers. Samples were examined using backscattered electron imagery, and selected minerals were quantitatively analysed. Elements analysed included F, Na, Mg, Al, Si, P, S, Cl, K, Ca, Ti, Cr, Mn, Fe, Sr and Ba. An accelerating voltage of 15 kV and probe current of 20 nA were used, except for analyses using general glass labels (i.e. chlorite), which utilised a 10 nA probe current. Peak count numbers of 20 s were used for all elements, except for F (40 s; amph/mica), F (60 s; glass), Cl (40 s), S (30 s), Sr (60 s) and Ba (60 s). Background count numbers were one-half the peak count times. A point beam of 1 μm was used to analyse amphibole, pyroxene, epidote, Fe–Ti oxide and zircon. A slightly defocused (10 μm) beam was used to analyse feldspar, mica and chlorite to avoid losses caused by sodium volatilisation (Nielsen & Sigurdsson, 1981). Analytical results are presented in Supplementary Table 1.

3.3 Radiogenic isotope analyses

Isotopic analyses of Sr, Nd and Pb were performed at the Department of Geological Sciences, New Mexico

State University. All isotopic measurements were made by TIMS, on a VG Sector 30 mass spectrometer. All samples analysed were loaded onto rhenium filaments on either Cathodian beads (single filament only) or on the side filament of a triple filament assembly. Reproducibility of the $^{87}\text{Rb}/^{86}\text{Sr}$ and $^{147}\text{Sm}/^{144}\text{Nd}$ ratios is within .3%, and the $^{87}\text{Sr}/^{86}\text{Sr}$ and $^{143}\text{Nd}/^{144}\text{Nd}$ ratios are within ± 0.00025 and ± 0.00003 , respectively. An analysis of the NBS 987 standard yielded values of .710226 (11), .710213 (13), .710219 (10) and .710260 (11). Pb samples were analysed using the middle filament position of a Cathodian bead assembly. Samples were loaded using 5% HNO_3 in a matrix of silica gel and phosphoric acid. Approximately 2 μL of silica gel was positioned on the filament and 1 μL of phosphoric acid was added. Standards were also loaded and analysed using the same procedures. The mean of standard runs was $^{206}\text{Pb}/^{204}\text{Pb} = 16.844$, $^{207}\text{Pb}/^{204}\text{Pb} = 15.379$ and $^{208}\text{Pb}/^{204}\text{Pb} = 36.199$. Deviations of the standards are within .2%. The detailed analytical procedures for Sr, Nd and Pb isotopic measurements are provided by Ramos (1992).

3.4 $^{40}\text{Ar}/^{39}\text{Ar}$ analyses

$^{40}\text{Ar}/^{39}\text{Ar}$ incremental heating experiments were carried out in New Mexico Geochronology Research Laboratory at the New Mexico Tech University, USA. Whole rock reacted with dilute HCl followed by DI water rinse in an ultrasound. Fragments picked were free of phenocrysts. Hornblende separated by standard magmatic, heavy liquid and picking techniques. Samples were loaded onto machined Al disc and irradiated for 8 h in the central thimble at the USGS reactor, Denver, CO. Neutron flux monitors Fish Canyon Tuff sanidine (FC-2). Assigned age = 28.201 Ma (Kuiper et al., 2008). ^{40}K Decay constant $5.643\text{e}-10/\text{a}$ (Min, Mundil, Renne, & Ludwig, 2000). Thermo-Fisher Scientific ARGUS VI mass spectrometer on line is used, with automated all-metal extraction system. System = Obama Multi-collector configuration: 40Ar-H1, 39Ar-Ax, 38Ar-L1, 37Ar-L2 and 36Ar-L3 Amplification: H1, L1, L2 1E12 ohm Faraday, AX 1E13 ohm Faraday, L3 – CDD ion counter, deadtime 14 nS. Laser Step-heating: Samples step-heated with 75W Photon-Machines 810 nm diode laser. Reactive gases removed by a 5-min reaction with 1 SAES GP-50 getters operated at 450 °C. Gas also exposed to cold finger operated at -140 °C and a W filament operated at ~2000 °C. Mass spectrometer sensitivity = $1\text{E}-16$ mol/fA. Total system blank and background: $60 \pm 5\%$, $.3 \pm 20\%$, $.1 \pm 50\%$, $.20 \pm 50\%$, $.22 \pm 5\%$, $\times 10^{-17}$ moles for mass numbers 40, 39, 38, 37 and 36, respectively. J-factors determined to a precision of $\sim \pm 0.04\%$ by CO_2 laser-fusion of six single crystals from each of six radial positions around the irradiation tray. Correction factors for interfering nuclear reactions were determined using K-glass and CaF_2 and are as follows: $(^{40}\text{Ar}/^{39}\text{Ar})_{\text{K}} = .0072 \pm .00002$; $(^{36}\text{Ar}/^{37}\text{Ar})_{\text{Ca}} = .0002724 \pm .0000002$; and $(^{39}\text{Ar}/^{37}\text{Ar})_{\text{Ca}} = .00069 \pm .000002$.

4. Results

4.1 Petrography

The modal mineralogy and common textural features of Late Cretaceous Hamsilos volcanic rocks are summarised in Table 1. The high-K calc-alkaline rocks are observed on the western side of the Inceburun Peninsula; whereas, the shoshonitic rocks crop out around the Sinop Peninsula (Figure 1). In the light of volcanic stratigraphy, the high-K calc-alkaline rocks are represented by basaltic lavas and dikes. The shoshonitic rocks are represented by volcanoclastics (breccias and tuffs) and lavas flow (pillow lavas and basaltic lavas). Basaltic lavas are dark grey and are generally observed as lava flows in limited areas. Around the Sinop Peninsula, brecciated volcanoclastics are interbedded with shoshonitic basalts form the basement. Basaltic lavas also contain visible pyroxene and brown mica crystals.

Petrographically, the high-K calc-alkaline volcanic rocks are composed of clinopyroxene, orthopyroxene, plagioclase and opaque minerals and display hyalomicroclitic porphyritic and glomeroporphyritic textures (Figure 3(a)–(f)). They include olivine and apatite as accessory phases. Plagioclase phenocrysts are generally euhedral and show normal zoning, albite twinning, sieved texture and overgrowth rim (Figure 3(b)–(d) and (f)). Some of these plagioclases contain clinopyroxene inclusions (Figure 3(f)). Euhedral or subhedral clinopyroxene phenocrysts show twinning, as well as resorbed rims and embayments (Figure 3(a), (d), and (e)). They also contain opaque mineral inclusions.

The shoshonitic volcanic rocks display microclitic porphyritic, glomeroporphyritic, microgranular and vesicular textures (Figure 3(a)–(f)), and comprise clinopyroxene + plagioclase + phlogopite + analcime \pm sanidine \pm olivine \pm Fe–Ti oxide \pm apatite. Clinopyroxene phenocrysts, including inclusions of opaque minerals and apatite, are euhedral and characterised by oscillatory zoning (Figure 4(a), (b) and (f)). Plagioclase phenocrysts are generally euhedral and show albite twinning. Some of the microlites are sanidine (Figures 4(c) and 3(d)). Phlogopites are observed as euhedral to anhedral crystals with inclusions of Fe–Ti oxide and rarely have resorbed rims and embayments (Figure 4(d) and (e)). Analcimes are mostly observed in groundmass. However, rare analcime (possibly derived from leucite) phenocrysts are rounded and six-sided (Figure 4(a) and (b)). Olivines are generally euhedral and iddingsitized along rims and cracks (Figure 4(a)). Apatites are abundant as subhedral crystals (Figure 4(f)). Zeolite, calcite and chlorite are common secondary minerals.

4.2 Mineral chemistry

4.2.1 Clinopyroxene

The mineral compositions of the Hamsilos volcanic rocks are listed in Supplementary Table 1. The clinopyroxenes observing as normally and reversally zoned

Table 1. Generalised mineral paragenesis and textural features of the Hamsilos volcanic rocks.

Area/age	Rock type	Facies	Sample no.	Common modal mineralogy								Common textures				
				Cpx	Opx	Pl	Phl	Ol	Sa	Anl	Op		Ap			
High-K calc-alkaline rocks Late Cretaceous	Basalt, Basaltic andesite	Basaltic	I-1	+		+					+		Microlitic porphyritic, hyalomicrolitic porphyritic, glomeroporphyritic			
			Lava	I-2	+	+	+		+		+	+				
		Breccia	I-3	+		+			+		+					
			I-4	+	+	+					+	+				
	Shoshonitic rocks Late Cretaceous	Tephrite	Basaltic	S-1	+		+				+			Microgranular porphyritic, glomeroporphyritic, vesicular		
				Lava	S-2	+					+	+			+	
			Trachy basalt	Pillow	S-3	+		+	+			+			+	+
					Lava	S-5	+				+	+				+
Shoshonitic rocks Late Cretaceous	Trachy basalt	Pillow	S-6	+		+					+	+	Microgranular porphyritic, glomeroporphyritic			
			Lava	S-7	+				+	+	+	+				
		Breccia	S-8	+		+						+	+			
			S-9	+			+		+	+	+	+	Microgranular porphyritic, glomeroporphyritic, fluidal, vesicular			
			S-10	+		+	+			+	+	+				
			S-11	+			+				+					
S-12	+			+		+	+	+	+							
			S-13	+			+		+	+	+					

crystals from the shoshonitic volcanic rocks are classified (Morimoto, 1988) as augite and diopside with $Wo_{42-49}En_{37-49}Fs_{4-17}$ and Mg number (Mg#) ranging from .69 to .92 (Figure 5(a), supplementary Table 1). Clinopyroxene is augite ($Wo_{41-44}En_{42-46}Fs_{11-17}$) in composition with Mg# ranging from .71 to .81 and orthopyroxenes are clinoenstatite ($Wo_{3-5}En_{65-67}Fs_{429-31}$) in compositions with Mg# varying from .67 to .70 from the high-K calc-alkaline volcanic rocks (Figure 5(a)).

The normally zoned clinopyroxenes are characterised by core composition with Mg-number varying from .71 to .92 in the shoshonitic, and .72–.81 in the high-K calc-alkaline rocks. The rim compositions range from .69 to .75 in the shoshonitic and .71 in the high-K calc-alkaline rocks, respectively. The reversely zoned clinopyroxenes have Mg-number in the core .71 for the shoshonitic and .71 for the high-K calc-alkaline rocks, and in the rim .73 for the shoshonitic and .81 for the high-K calc-alkaline rocks. Orthopyroxenes do not show zoning in the high-K calc-alkaline volcanic rocks.

4.2.2 Feldspar

Plagioclase phenocrysts in Hamsilos shoshonitic volcanic rocks comprise broad compositions ranging from andesine to bytownite (An_{48-84}). K-feldspar phenocrysts are sanidine (Or_{40-98}).

Microlites in groundmass appear as labradorite to bytownite with An_{60-84} and sanidine (Or_{48-98}) (Figure 5(b)). While the core compositions of normally zoned plagioclases are An_{76-81} for the shoshonitic rocks and An_{76-81} for the high-K calc-alkaline rocks, the rim compositions of these rocks are An_{56-67} and An_{65-76} , respectively. Plagioclases from the high-K calc-alkaline

volcanic rocks are characterised by labradorite and bytownite (An_{65-86}) (Figure 5(b)).

4.2.3 Brown mica

The Mg# of brown micas varies from .61 to .66 for the shoshonitic volcanic rocks. Brown micas are classified as the phlogopite (Speer, 1984) (Figure 5(c)).

4.2.4 Analcime

Euhedral to subhedral analcimes in the Hamsilos shoshonitic volcanic rocks present high contents of Na_2O (10–13 wt%) and low contents of K_2O (0–1 wt%).

4.2.5 Fe–Ti oxide

Fe–Ti oxides generally possess similar compositions in the Hamsilos volcanic rocks. These Fe–Ti oxides are magnetite and titanomagnetite (Figure 5(d)).

4.3 Intensive parameters

4.3.1 Clinopyroxene thermobarometry

The temperature, pressure and crystallisation depth of volcanic rocks can be estimated on the basis of clinopyroxene composition (Nimis, 1995; Nimis & Taylor, 2000; Nimis & Ulmer, 1998) and clinopyroxene–liquid equilibria (Putirka, 2008; Putirka, Johnson, Kinzler, & Longhi, 1996; Putirka, Mikaelian, & Ryerson, 2003). Putirka (2008) re-evaluated many quantitative temperature and pressure estimates on clinopyroxene composition and obtained an equilibrium constant using Fe–Mg

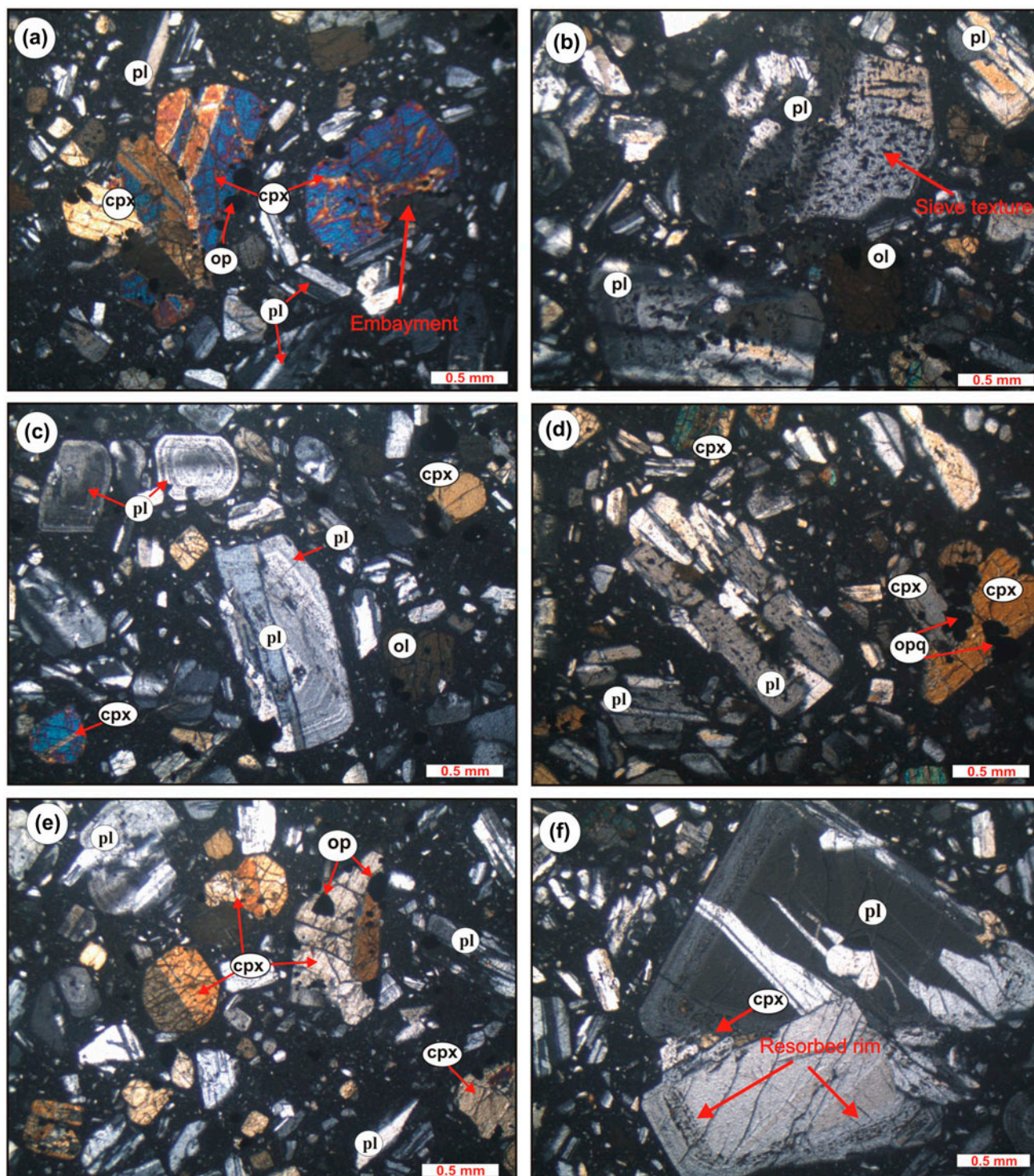


Figure 3. Microphotographs of the Hamsilos high-K calc-alkaline volcanic rocks (a) twinned clinopyroxene phenocryst with embayed in glomeroporphyritic texture, (b) sieve texture and overgrowth rim in plagioclase and anhedral olivine, (c) normal zoning, sieve texture and oscillatory zoned plagioclase phenocryst, (d) and (e) albite twinning, sieved texture and opaque mineral inclusions in zoned clinopyroxene, (f) opaque inclusions in resorbed rim plagioclase, clinopyroxene in microgranular porphyritic texture (cpx: clinopyroxene, pl: plagioclase, ol: olivine, op: Fe-Ti oxide, crossed polarized light).

exchange and $K_D(\text{Fe-Mg})^{\text{cpx-liq}} = .28 \pm .08$. The clinopyroxene thermobarometry-yielded temperature ranges from 1133 to 1187 °C for clinopyroxenes from the shoshonitic volcanic rocks and from 1004 to 1174 °C

for the high-K calc-alkaline volcanic rocks. The estimated crystallisation pressures of clinopyroxenes range from 1.4 to 6.3 kbar for the shoshonitic volcanic rocks and from 1.5 to 3.6 kbar for the high-K calc-alkaline

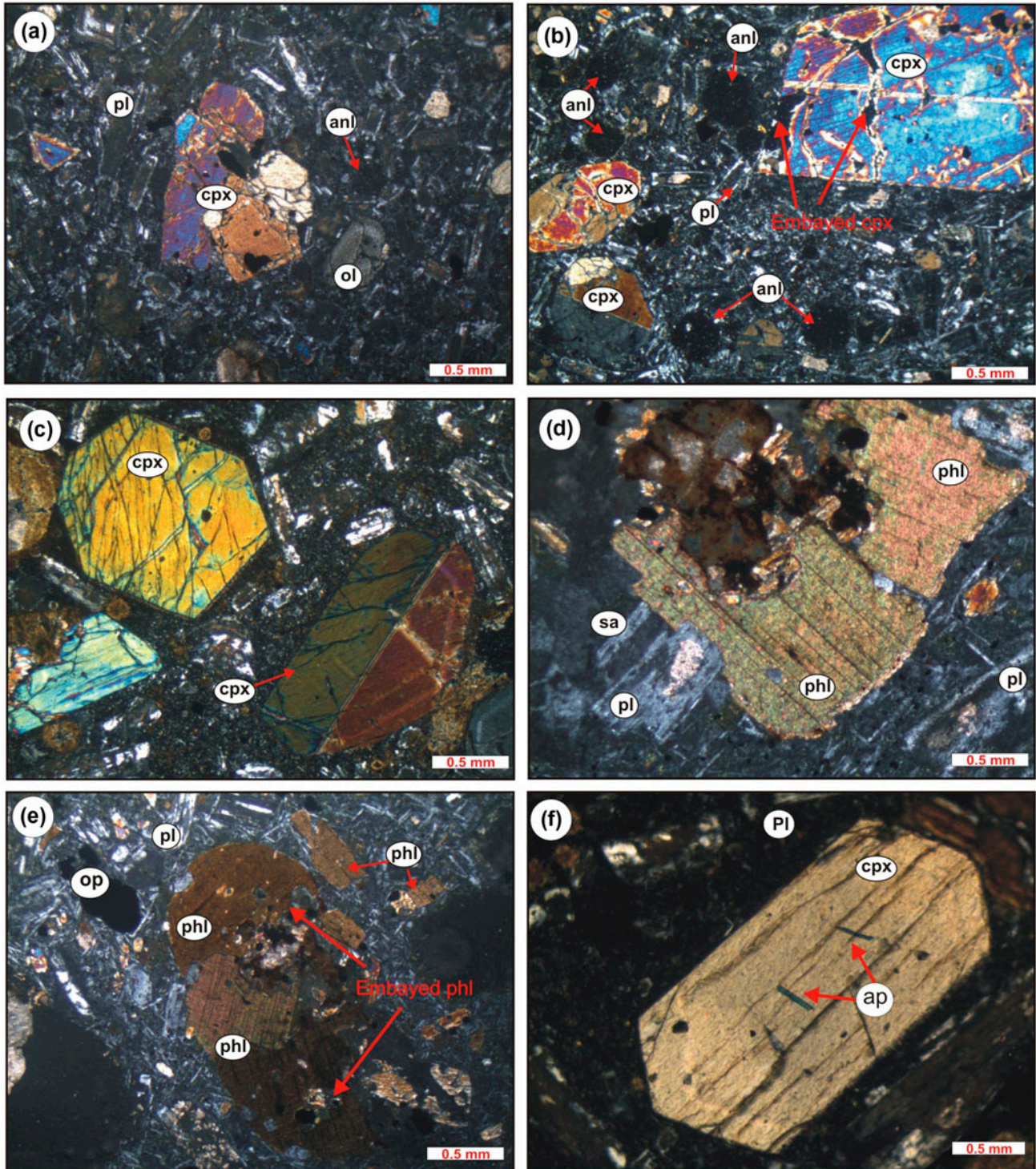


Figure 4. Microphotographs of the Hamsilos shoshonitic volcanic rocks (a) analcime phenocryst, plagioclase and clinopyroxene in glomeroporphyritic texture, (b) resorbed rim and zoning in clinopyroxenes, euhedral analcime and plagioclase in microlitic-porphyritic texture, (c) embayed and zoned clinopyroxene in glassy groundmass, (d) lath-shaped and microlites sanidine, plagioclase and brown mica phenocryst with characteristic cleavage, (e) embayed phlogopite, plagioclase and opaque in glomeroporphyritic texture, (f) apatite mineral inclusion in clinopyroxene (cpx: clinopyroxene, pl: plagioclase, anl: analcime, phl: phlogopite, sa: sanidine, ol: olivine, op: Fe–Ti oxide, ap: apatite, crossed polarized light).

volcanic rocks. These pressures obtained using clinopyroxene barometer correspond to crystallisation depths of 6–18 and 5–12 km, respectively (Table 2).

4.3.2 Biotite thermobarometry and oxygen fugacity

The empirical equation proposed by Uchida, Endo, and Makino (2007) was used to estimate the crystallisation

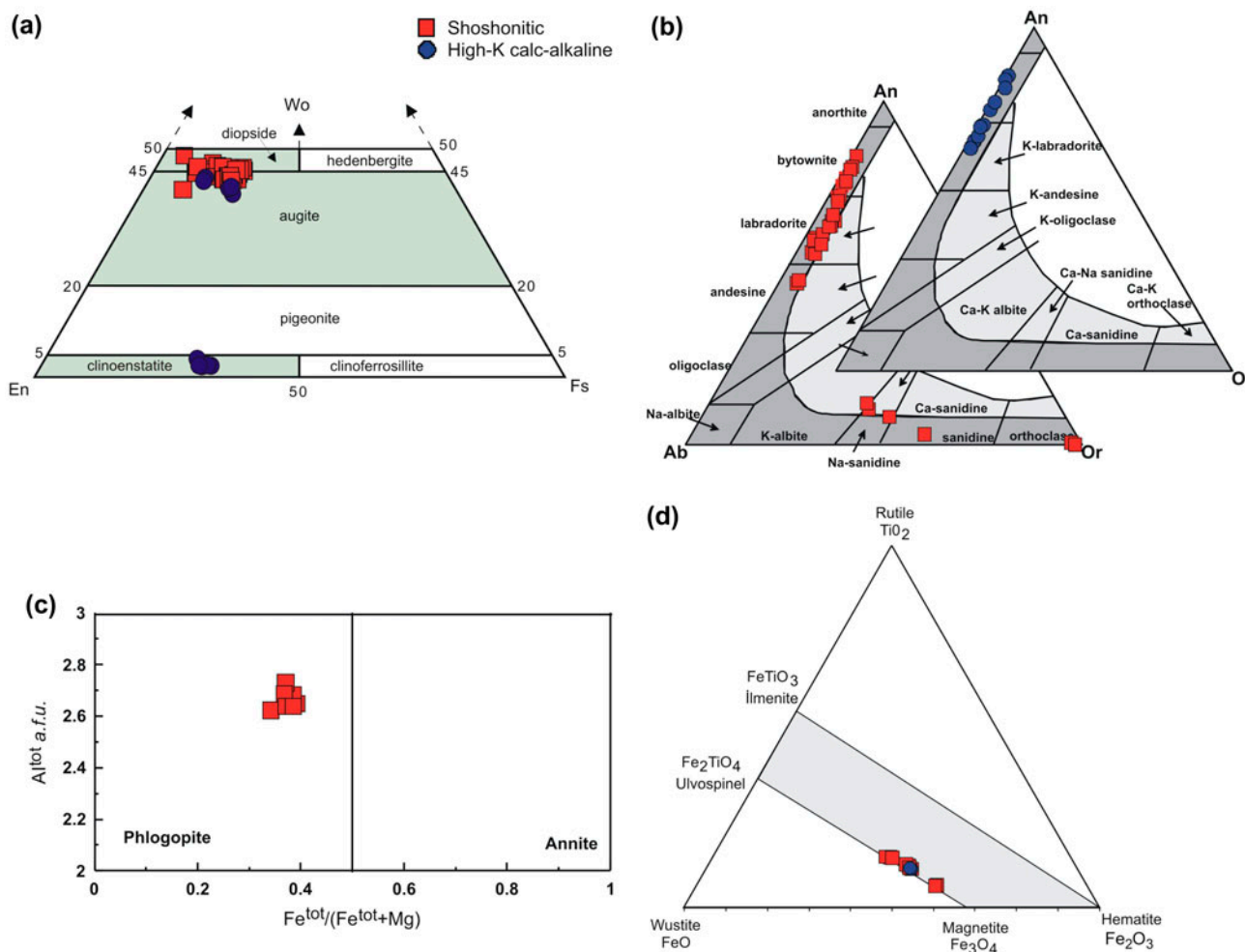


Figure 5. (a) Clinopyroxene classification diagram (Morimoto, 1988), (b) An–Ab–Or triangular plot showing the compositions of feldspars, (c) the biotite classification diagram of Spear (1984), (d) Plot of Fe–Ti oxides in the ternary TiO_2 –FeO– Fe_2O_3 diagram (Bacon & Hirschmann, 1988) for the studied volcanics.

pressures for the studied volcanics. The equation was calibrated using the Al^{tot} (total aluminum) content in biotite on the basis of 11 oxygens. The calculated mean pressure is 1.41–1.71 kbar (mean = 1.54 ± 0.10 kbar) for the shoshonitic volcanic rocks (Table 3). The mean crystallisation temperature was calculated using the formula of Luhr, Carmichael, and Varekamp (1984) as range from 724.68 to 993.46 °C (mean = 804.18 ± 90.20 °C), for the shoshonitic volcanic rocks (Table 3). The proposed quantitative estimation of oxygen fugacity by Wones and Eugster (1965) was tested using the biotite temperature (Luhr et al., 1984) and pressure (Uchida et al., 2007) values obtained for the studied rocks. The calculated mean oxygen fugacity condition is between 16.02 and 9.44 (mean = 13.89 ± 2.19) for the shoshonitic volcanic rocks (Table 3).

4.4 $^{40}Ar/^{39}Ar$ dating

The results of Ar–Ar dating are given in Table 4. Age spectras for three biotite separates and a whole-rock

sample are shown in Figure 6. Three Hamsilos shoshonitic samples (S-1, S-3, and S-5) yielded $^{40}Ar/^{39}Ar$ plateau ages of 79.0 ± 0.3 , 77.3 ± 0.4 and 78.2 ± 0.7 Ma, respectively. A high-K calc-alkaline sample (I-6) yielded a $^{40}Ar/^{39}Ar$ age of 72.3 ± 0.5 Ma (Figure 6 and Table 4), which corresponds to the Late Cretaceous period (Campanian). Asan et al. (2014) reported that two Hamsilos shoshonitic samples yielded $^{40}Ar/^{39}Ar$ plateau ages of 82.08 ± 1.13 and 81.37 ± 0.4 Ma and a high-K calc-alkaline sample yielded a $^{40}Ar/^{39}Ar$ age of 82.18 ± 0.41 Ma.

4.5 Whole-rock geochemistry

4.5.1. Effects of the alteration and analcimization

The analytic results showed that the LOI values of the Hamsilos volcanic rock samples vary in the range of 2.8–6.7 wt% for the shoshonitic rocks, and .4–1.0 wt% for the high-K calc-alkaline rocks (Table 5). The shoshonitic rocks which have high LOI values are likely related to alterations (chemical or weathering) or analcimization

Table 2. Termobarometry and temperature calculations from the clinopyroxene chemistry of the Hamsilos volcanic rocks.

Clinopyroxene – only thermobarometer (Putirka, 2008)			
Hamsilos volcanic rocks	$K_D(\text{Fe-Mg})^{\text{cpx-liq}} = .28 \pm .08$	Eqn 32b (kbar)	Eqn 32d ($^{\circ}\text{C}$)
	<i>Shoshonitic rocks</i> ($n = 21$)	Core	
	Mean	4.4 ± 1.2	1168 ± 18.5
	Max	6.3	1187.2
	Min	1.4	1133.4
	<i>High-K calc-alkaline</i> ($n = 3$)	Eqn 32a (kbar)	Eqn 32d ($^{\circ}\text{C}$)
	Mean	2.5 ± 1.1	113.6 ± 95
	Max	3.6	1004.3
	Min	1.5	1174.3

Table 3. Biotite temperature, pressure and oxygen fugacity calculations for the studied volcanics.

Biotite thermobarometers and oxygen fugacity				
Hamsilos volcanic rocks	Shoshonitic rocks ($n = 7$)	Luhr et al. (1984) (T $^{\circ}\text{C}$)	Uchida et al. (2007) (P kbar)	Wones and Eugster (1965) ($f\text{O}_2$)
	Mean	804.18 ± 90.20	$1.54 \pm .10$	-13.89 ± 2.19
	Max	993.46	1.71	-9.44
	Min	724.68	1.41	-16.02

of the leucite. Therefore, several geochemical parameters have been used to test the effects of alteration and weathering processes; the Weathering Index of Parker (WIP; Parker, 1970), Chemical Index of Alteration (CIA; Nesbitt & Young, 1982) parameters have been calculated, and rocks having WIP values (70–100) close to 100, with CIA values (33–46) lower than 50 (Table 5), are considered to have been unaffected by weathering and/or alteration processes (Ersoy & Helvacı, 2016; Kasapoğlu et al., 2016). MFW plot of Ohta and Arai (2007) was also used to fresh magmatic rocks follow a ‘magmatic trend’, and all of the Hamsilos volcanic rocks lie along this trend (Figure 7(a)). In case of the data for the Hamsilos volcanics (Asan et al., 2014), only three samples fall off the trend and it has been excluded from following sections.

According to this result, the relatively high LOI value ranges from 2.8 to 6.7 wt% for the shoshonitic rocks is mainly due to the presence of analcime phenocrysts (analcimisation). Although the replacement of leucite by analcime is common on potassic rocks in older ages, the origin of these analcimes is matter of debate (Asan et al., 2014; Eyüboğlu, 2010; Varol, 2013; Yücel, Temizel, Abdioğlu, Arslan, & Yağcıoğlu, 2014). There are two ideas in order to explain whether or not the analcimes primary or secondary; (1) the analcimes in these rocks are primary, but the presence of analcimes as primary occurrences is very limited (e.g. Luhr & Kyser, 1989; Pearce, 1993), (2) transformation of analcimes from pre-existing mineral phases as leucite, nepheline (e.g. Gupta & Fyfe, 1975; Karlsson & Clayton, 1991; Putnis, Putnis, & Giampaolo, 1994; Moradian, 2008). Moreover, the higher Fe content of analcime ($\text{Fe} > .025$) can be accepted as a distinguishing evidence for primary origin by Luhr and Kyser (1989). The analcimes in

shoshonites of Hamsilos volcanic rocks are possibly derived from leucite with a low Fe content of analcimes. The fresh character of host rocks and the absence of hydrous minerals such as amphibole and phlogopite according to Karlsson and Clayton (1991) are supporting the idea of secondary origin of analcimes in shoshonites. Additionally, the primary crystallisation of analcime required the crystallisation other Na-bearing phases as Na-pyroxenes instead of augite and diopside present in shoshonites of Hamsilos volcanic rocks.

4.5.2. Major and trace elements

Representative results of geochemical compositions for Hamsilos volcanic rocks are presented in Table 5. SiO_2 content varies from 46.64 to 51.51 wt% for shoshonitic rocks and from 53.79 to 54.55 wt% for high-K calc-alkaline rocks. Mg# values range between 48 and 62 (Table 5). Both lava types have contents of Al_2O_3 (14.77–18.51 wt%), K_2O (1.36–5.38 wt%), Na_2O (2.50–3.62 wt%), Fe_2O_3^* (7.30–8.66 wt%) and low TiO_2 (<1.0 wt%). The relatively high LOI values of the shoshonitic samples (2.8–6.7 wt%) are related to their glassy texture and secondary minerals (zeolite and calcite inclusions) as well as the presence of analcime minerals (analcimisation) and minor primary hydrous phases, such as phlogopite. Besides, the shoshonitic rocks contain normative nepheline and olivine revealing silica undersaturated compositions (Table 5). The normative nepheline is consistent with modal analcime contents of the shoshonitic rocks.

In the SiO_2 vs. $\text{Na}_2\text{O} + \text{K}_2\text{O}$ diagram (TAS) of (Le Bas, Le Maitre, Streckensen, & Zanettin, 1986), high-K calc-alkaline volcanic rocks fall into the basaltic andesite field, whereas shoshonitic volcanic samples fall into the

Table 4. ³⁹Ar/⁴⁰Ar age spectra of four volcanic rock samples (A, B, C: shoshonite, D: high-K basaltic andesite) from the Hamsilos volcanic rock.

ID	Power (Watts)	⁴⁰ Ar/ ³⁹ Ar	³⁷ Ar/ ³⁹ Ar	³⁶ Ar/ ³⁹ Ar ($\times 10^{-3}$)	³⁹ ArK ($\times 10^{-15}$ mol)	K/Ca	⁴⁰ Ar* (%)	³⁹ Ar (%)	Yaş (Ma)	± 1 sigma (Ma)
S-1, biotite, 3.94 mg, $J = .0013552 \pm .03\%$, IC = 1.01828 \pm .00093, NM-262G, Lab# = 62165-01										
A	1	78.08	2.055	138.9	.368	.25	47.6	21.7	90.01	.56
B	1.8	72.92	1.033	136.8	.26	.49	44.7	37	78.99	.62
C	2.3	35.95	.9756	9.924	.181	.52	92.1	47.7	80.23	.71
D	2.5	36.59	1.639	14.27	.149	.31	88.8	56.5	78.87	.86
E	3	36.06	3.928	13.51	.181	.13	89.8	67.2	78.71	.77
F	3.5	40.94	3.262	35.14	.056	.16	75.3	70.5	74.9	2.2
G	4	35.4	4.848	6.491	.032	.11	95.7	72.4	82.3	4.3
H	4.5	38	12.68	21.56	.047	.04	85.9	75.1	79.8	2.7
I	5	36.51	8.527	14.14	.025	.06	90.4	76.6	80.5	5.2
J	6	36.79	27.81	28.56	.044	.018	83.1	79.1	75.6	2.9
K	8	43.37	74.59	63	.139	.007	70.9	87.3	78.6	.94
L	21	45.36	313.3	148.9	.215	.002	58.6	100	82.1	.81
Integrated age ± 1 s		$n = 12$			1.697			K ₂ O = .12%	81.7	.3
Plateau age ± 1 s		Steps B-K $n = 10$	MSWD = .99		1.114			65.6	79.04	.33
S-3, biotite, 4.92 mg, $J = .001355 \pm .03\%$, IC = 1.01828 \pm .00093, NM-262G, Lab# = 62164-01										
A	1	228.9	.3728	631.6	.519	1.4	18.5	8.1	102.09	.78
B	1.8	65.12	.3623	113.4	.602	1.4	48.6	17.5	76.83	.33
C	2.3	42.66	.4535	37.19	.719	1.1	74.3	28.7	77.01	.22
D	2.5	45.76	.9432	49.25	.643	.54	68.4	38.7	76.02	.26
E	3	38.35	2.011	21.65	1.055	.25	83.7	55.1	78.06	.16
F	3.5	40.22	2.982	28.35	1.523	.17	79.8	78.8	78.04	.12
G	4	48.47	7.658	60.73	1.289	.067	64.2	98.9	76.02	.15
H	4.5	36.77	8.994	25.59	.074	.057	81.4	100	73.2	1.6
Integrated age ± 1 s		$n = 8$			6.42			K ₂ O = .37%	79.11	.11
Plateau age ± 1 s		Steps B-H $n = 7$	MSWD = 28.24	5.905		.18		91.9	77.29	.37
S-5, biotite, 4.3 mg, $J = .0013578 \pm .04\%$, IC = 1.01828 \pm .00093, NM-262G, Lab# = 62168-01										
A	1	112.3	1.576	296.1	.164	.32	22.2	28.6	60.99	.94
B	1.8	116	.2642	281.5	.127	1.9	28.3	45.6	79.8	1.3
C	2.3	38.59	.6139	23.65	.074	.83	82	54.2	77	1.7
D	2.5	41.74	.9792	26.41	.043	.52	81.5	58.6	82.7	3.1
E	3	37.38	1.536	13.61	.062	.33	89.6	64.7	81.4	2.1
F	3.5	36.96	2.149	16.73	.051	.24	87.1	69.3	78.4	2.5
G	4	37.95	3.376	22.78	.046	.15	83	73.1	76.8	2.7
H	4.5	37.1	3.583	12.33	.044	.14	91	76.6	82.2	2.9
I	5	34.4	4.291	9.214	.067	.12	93.1	81.6	78.1	1.9
J	6	44.65	13.11	49.15	.098	.039	69.8	88.3	76.6	1.3
K	8	37.07	90.98	52.03	.087	.006	78.3	93.5	75.4	1.5
L	21	42.39	481.3	196.8	.119	.001	54.2	100	83.5	1.4
Integrated age ± 1 s		$n = 12$.983			K ₂ O = .06%	76.1	.5
Plateau age ± 1 s		Steps B-K $n = 10$	MSWD = 1.53	.7		.55 \pm .58		71.2	78.18	.72

(Continued)

Table 4. (Continued).

ID	Power (Watts)	$^{40}\text{Ar}/^{39}\text{Ar}$	$^{37}\text{Ar}/^{39}\text{Ar}$	$^{36}\text{Ar}/^{39}\text{Ar}$ ($\times 10^{-3}$)	^{39}ArK ($\times 10^{-15}$ mol)	K/Ca	$^{40}\text{Ar}^*$ (%)	^{39}Ar (%)	Yaş (Ma)	± 1 sigma (Ma)
I-6, whole-rock, 4.41 mg, $J = .0013625 \pm .04\%$, $IC = 1.01828 \pm .00093$, NM-262G, Lab# = 62171-01										
A	1	2998.1	23.29	10051.5	.175	.022	1	4.6	73.9	7.8
B	2	321.6	35.29	990.1	.27	.014	9.9	11.6	79.6	1.3
C	3	240.2	33.3	712.8	.345	.015	13.4	20.7	80.6	.95
D	4	151.8	30.84	419.8	.395	.017	19.9	31	75.53	.68
E	5	122.5	29.77	320.9	.377	.017	24.5	40.9	74.93	.64
F	6	98.86	29.07	242.3	.414	.018	29.9	51.7	73.82	.54
G	7	59.6	27.64	114.1	.306	.018	47.2	59.7	70.12	.52
H	8	52.31	24.21	89.41	.298	.021	53.2	67.5	69.26	.49
I	9	40.56	18.07	55.45	.233	.028	63.2	73.6	63.59	.54
J	10	30.77	14.2	33.84	.175	.036	71.2	78.2	54.37	.6
K	12	32.37	13.62	38.5	.168	.037	68.2	82.6	54.76	.62
L	21	40.95	19.12	41.78	.665	.027	73.6	100	72.3	.5
Integrated age ± 1 s					3.82			$K_2O = .24\%$	71.24	.4
Plateau age ± 1 s		No plateau								

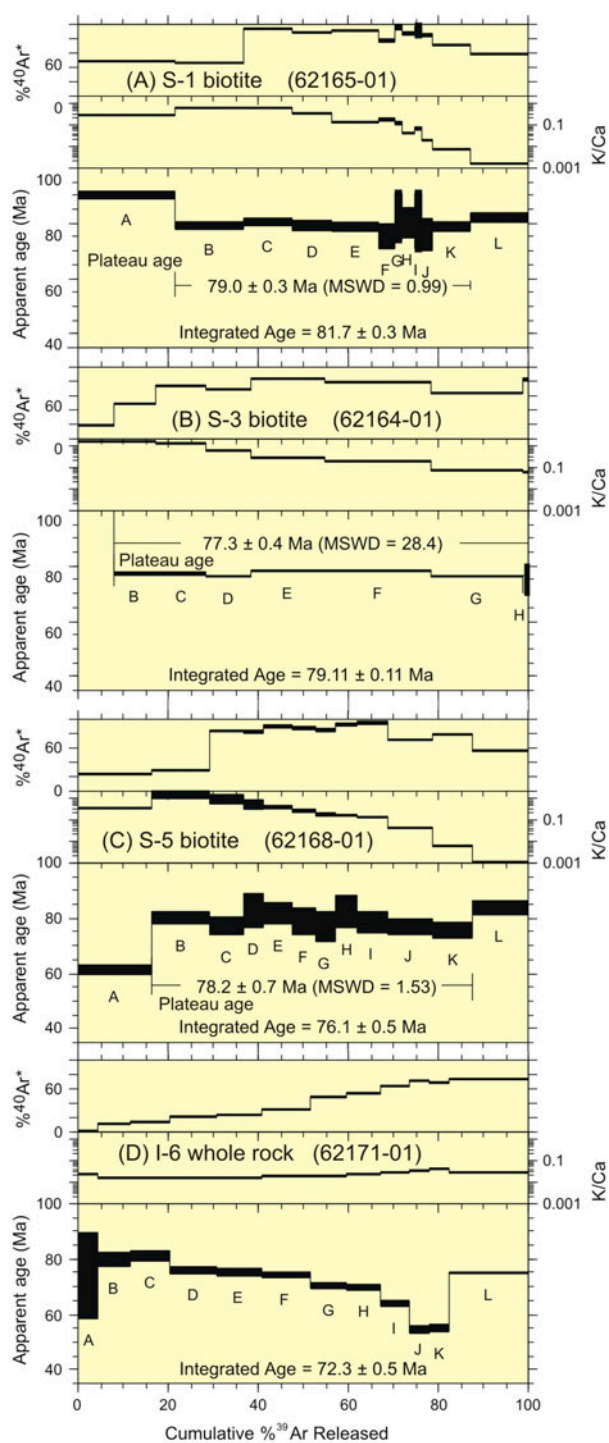


Figure 6. $^{40}\text{Ar}/^{39}\text{Ar}$ age spectra of four volcanic rock samples (A, B, C: shoshonite, D: high-K basaltic andesite) from the Hamsilos volcanic rock. MSWD: mean square of the weighted deviates.

trachy-basalt, basaltic trachy andesite and phono-tephrite fields (Figure 7(b)). In the chemical classification diagram of Hastie, Kerr, Pearce, and Mitchell (2007), the high-K calc-alkaline samples fall into the calc-alkaline field, while those from the shoshonitic samples are plotted on the high-K and shoshonitic fields (Figure 7(c)). In a K_2O vs. Na_2O diagram, high-K calc-alkaline rocks fall

into the calc-alkaline field, but shoshonitic samples are plotted in the shoshonitic field (Figure 7(d)).

The SiO_2 vs. major and trace element variation diagrams of Hamsilos volcanic rocks generally exhibit negative or positive correlation with various scattering (Figure 8). An increase in the SiO_2 content of Hamsilos volcanites displays decrease in CaO , MgO , TiO_2 , Ni and Sr content and an increase in Al_2O_3 , $\text{Fe}_2\text{O}_3(\text{t})$, P_2O_5 , Zr , Rb and Ba content. Although K_2O and Na_2O show scatter, they display increasing trend with SiO_2 (Figure 8). Degreasing CaO with increasing SiO_2 shows clinopyroxene and plagioclase fractionation. The scatter of K_2O and Na_2O for the samples could be related to analcimization of the leucite within these rocks. P_2O_5 content shows opposite behaviour in the high-K calc-alkaline and shoshonitic volcanic rocks. These variations can be explained by the fractionation of common mineral phases, such as plagioclase + clinopyroxene \pm biotite \pm Fe-Ti oxide \pm apatite in shoshonitic rocks and plagioclase + clinopyroxene \pm olivine \pm Fe-Ti oxide in high-K calc-alkaline rocks.

Hamsilos volcanic rocks are enriched in large-ion lithophile (LILE) elements and light rare earth elements (LREEs) relative to high-field-strength elements (HFSEs) (Figure 9(a)–(d)). The primitive mantle normalised multi-element variation diagrams of the studied samples show enrichment in LILE (e.g. Rb , Th , and K) relative to HFSE and also negative Nb , Ta and Ti anomalies (Figure 9(a) and (b)). These characteristics are typical of subduction-related magma (Elliott, Plank, Zindler, White, & Bourdon, 1997; Gill, 1981; Hofmann, 1997; Pearce et al., 1990; Tatsumi, Hamilton, & Nesbitt, 1986). However, compared to those derived from depleted mantle, slight enrichment in LILE and decrease in negative Nb , Ta and Ti anomalies can be ascribed to the some contribution of melts from asthenosphere to the mantle wedge. Although the trace element variations in shoshonitic and high-K calc-alkaline samples are similar to each other, there is a systematic increase in the trace element concentrations from the high-K calc-alkaline lavas to the shoshonitic lavas (Figure 9(a) and (b)). The trace element compositions of the Hamsilos volcanic rocks are generally similar to the Ultra-K and shoshonitic rocks in Asan et al. (2014) and the Ultra-K and shoshonitic rocks from the eastern Pontides (Altherr et al., 2008; Asan et al., 2014; Eyüboğlu, 2010; Gülmez & Genc, 2015).

Chondrite-normalised (Boynton, 1984) REE patterns (Figure 9(c) and (d)) for the shoshonitic and high-K calc-alkaline samples display enrichment in LREEs relative to HREE. The field of REE abundances of samples from the Hamsilos volcanics is also shown for comparison that the previous study by Asan et al. (2014) has slightly higher abundances of LREE and HREE. The shoshonitic and high-K calc-alkaline samples show moderately fractionated chondrite-normalised REE patterns subparallel to each other with $(\text{La}/\text{Lu})_{\text{N}}$ of 7.47–16.7 and 5.75–6.70, respectively. REE distributions also have characteristic concave patterns in shoshonitic and high-K

Table 5. Whole-rock major element oxide (wt%), CIPW norms, trace and rare earth elements (ppm) and weathering/alteration indexes (CIA and WIP) of the Hamsilos volcanic rocks.

Sample no.	Shoshonitic													Hig-K calc-alkaline						
	S-1	S-2	S-3	S-5	S-6	S-7	S-8	S-9	S-10	S-11	S-12	S-13	I-6	I-7	I-1	I-2	I-3	I-4	I-5	I-8
SiO ₂	49.2	50.4	49.9	48.1	49.8	51.5	50.1	47.9	49.7	50.7	48.3	46.6	53.8	54.3	54.3	54.2	54.3	54.4	54.0	54.6
TiO ₂	.870	.800	.620	.880	.880	.830	.630	.860	.880	.790	.600	.840	.580	.580	.570	.580	.580	.580	.580	.570
Al ₂ O ₃	15.3	16.7	17.0	15.0	15.9	17.2	17.0	14.8	15.8	16.9	16.5	14.8	18.3	18.2	18.3	18.3	18.3	18.4	18.5	18.5
Fe ₂ O ₃	7.84	7.49	7.65	7.48	8.66	7.44	7.88	7.66	7.49	7.57	7.36	7.3	8.34	8.24	8.47	8.41	8.36	8.58	8.32	8.12
MnO	.140	.130	.150	.160	.120	.120	.150	.160	.130	.140	.180	.180	.150	.150	.150	.150	.150	.160	.150	.150
MgO	4.59	4.65	3.62	5.9	5.05	4.74	3.72	6.27	4.4	4.58	3.52	5.6	4.54	4.6	4.51	4.41	4.4	4.48	4.54	4.55
CaO	9.46	7.99	7.08	11.6	8.78	7.74	6.94	11.92	9.1	7.94	8.7	12.75	8.86	8.7	8.64	8.64	8.56	8.71	8.78	8.74
Na ₂ O	3.54	2.50	2.69	2.56	3.49	2.55	2.76	2.51	3.62	2.54	2.63	2.50	2.60	2.60	2.56	2.57	2.53	2.67	2.57	2.61
K ₂ O	2.65	4.25	5.26	2.73	2.48	4.48	5.38	2.64	2.62	4.2	4.95	2.63	1.47	1.49	1.45	1.39	1.48	1.36	1.45	1.46
P ₂ O ₅	.300	.300	.340	.250	.300	.310	.340	.240	.290	.290	.320	.240	.140	.140	.140	.110	.120	.110	.120	.120
LOI	5.80	4.40	5.50	5.10	4.20	2.80	4.80	4.80	5.80	4.10	6.70	6.20	1.00	.800	.700	1.00	1.00	.500	.700	.400
Sum	99.7	99.7	99.7	99.7	99.7	99.7	99.7	99.7	99.7	99.7	99.7	99.7	99.8	99.8	99.8	99.8	99.8	99.8	99.8	99.8
K/Na	.7	1.7	2.0	1.1	.7	1.8	1.9	1.1	.7	1.7	1.9	1.1	.6	.6	.6	.5	.6	.5	.6	.6
Ni	10.6	14.0	11.1	21.3	14.0	12.5	11.7	20.0	11.4	15.3	12.9	20.5	5.2	5.4	4.5	5.2	4.6	4.8	4.6	4.6
Sc	31.0	24.0	14.0	39.0	30.0	24.0	15.0	37.0	29.0	22.0	13.0	34.0	26.0	26.0	25.0	25.0	24.0	24.0	25.0	25.0
Ba	447	581	552	324	452	633	547	335	399	555	495	315	357	356	338	371	356	340	338	325
Co	19.1	22.5	19.0	27.9	27.4	23.8	20.6	31.1	17.9	24.7	17.3	27.1	23.9	23.8	22.4	22.9	23.4	21.4	23.5	22.0
Hf	4.30	5.30	5.50	3.10	4.50	5.50	5.50	2.90	4.50	5.20	5.30	2.90	2.10	2.10	2.00	2.10	2.10	2.20	2.00	2.10
Nb	8.50	12.80	16.00	6.70	8.90	13.60	16.30	7.10	7.50	11.80	14.10	6.50	3.40	3.40	3.00	3.00	2.90	3.10	3.00	3.10
Rb	38	144	141	87	35	157	149	89	35	137	125	81	50	52	48	52	53	45	49	50
Sr	371	484	393	560	379	528	422	562	363	504	395	553	339	341	326	341	333	321	333	332
Ta	.600	.900	1.000	.400	.500	.900	1.000	.400	.400	.700	.900	.400	.200	.200	.200	.200	.200	.200	.200	.200
Th	12.3	16.9	22.4	7.10	12.9	19.5	23.6	6.90	11.2	16.9	19.9	6.70	6.20	6.20	5.90	5.60	5.90	5.80	6.10	5.70
U	2.70	4.00	5.60	2.50	1.90	3.40	5.40	2.30	3.00	3.60	4.80	2.40	2.80	2.30	2.10	2.00	2.10	2.30	2.30	1.80
V	267	190	150	274	288	206	169	284	270	192	143	274	225	239	220	219	222	220	218	220
Zr	159.3	189.7	222.1	108.6	160	202.2	231.8	109.8	153.6	181.4	205.8	100.3	73.7	77.1	75.2	79.5	75.1	76.6	77.4	77.2
Y	22.6	22.8	26.1	22.2	22.6	22.6	25.9	21.4	20.8	20.6	24.3	20.5	15.8	15.6	14.2	14.8	15.3	15.4	16.3	15.2
Cu	76.3	57.1	72.8	136.1	46.7	42.9	73.1	114.7	69.9	63.1	84	143.3	102.1	98.1	92	84	65.3	109.4	101	81.8
Pb	4.90	7.20	5.50	4.40	2.10	5.80	3.20	3.70	5.10	9.40	4.40	5.20	3.50	1.90	3.90	5.50	2.50	2.90	2.40	1.70
Zn	50.0	66.0	67.0	63.0	71.0	71.0	75.0	57.0	55.0	75.0	63.0	61.0	25.0	34.0	36.0	39.0	23.0	38.0	29.0	21.0
Quartz	.00	.00	.00	.00	.00	.00	.00	.00	.00	.00	.00	.00	.00	.00	.00	.00	.00	.00	.00	.00
Anorthite	17.88	21.87	18.69	21.24	20.50	22.31	18.13	21.24	19.01	22.17	18.65	21.42	33.89	33.56	34.12	34.17	34.01	34.01	34.54	34.25
Albite	23.59	21.15	16.88	14.36	27.49	21.58	16.49	13.02	26.18	21.49	10.69	8.70	22.00	22.00	21.66	21.75	21.41	21.41	21.75	22.09
Orthoclase	15.81	25.12	31.08	16.13	14.66	26.48	31.79	15.60	15.48	24.82	29.25	15.54	8.69	8.81	8.86	8.50	9.04	9.04	8.86	8.92
Nepheline	3.45	.00	3.19	3.96	1.11	.00	3.72	4.45	2.41	.00	6.26	6.75	.00	.00	.00	.00	.00	.00	.00	.00
Leucite	.00	.00	.00	.00	.00	.00	.00	.00	.00	.00	.00	.00	.00	.00	.00	.00	.00	.00	.00	.00
Diopside	22.07	12.79	11.61	27.88	17.10	11.37	11.50	29.19	19.63	12.42	18.32	32.41	7.45	7.07	6.62	6.59	6.35	6.35	6.79	6.86
Hypersihene	.00	1.03	.00	.00	.00	1.91	.00	.00	.00	2.14	.00	.00	14.58	14.83	15.05	14.74	14.79	14.79	14.88	14.70
Olivine	4.85	7.31	6.96	5.00	7.92	7.25	7.32	5.35	5.11	6.59	4.26	2.84	.00	.00	.00	.00	.00	.00	.00	.00
Ilmenite	1.65	1.52	1.18	1.67	1.67	1.58	1.20	1.63	1.67	1.50	1.14	1.60	1.10	1.10	1.08	1.10	1.10	1.10	1.10	1.08
Magnetite	3.41	3.26	3.33	3.25	3.77	3.23	3.42	3.33	3.26	3.29	3.20	3.18	3.62	3.58	3.68	3.65	3.64	3.64	3.62	3.54
Apatite	.70	.70	.79	.58	.70	.72	.79	.56	.67	.67	.74	.56	.32	.32	.25	.25	.28	.28	.28	.28
Zircon	.01	.00	.00	.00	.00	.00	.00	.00	.00	.00	.00	.00	.00	.00	.01	.01	.01	.01	.01	.01
La	35.00	44.80	57	22.3	35.6	46.3	59	23.6	32.7	45	54.5	23	14.5	15.4	14.5	14.7	14.2	15	14.4	15.1
Ce	78.80	93.00	115.5	50.6	75.8	94.4	114.3	50.3	73	92.9	109	49.7	30.7	30.4	29	28.3	28.5	29	28.4	29.4
Pr	8.94	10.26	12.37	5.98	9.18	10.8	12.7	6.13	8.47	10.12	11.31	5.88	3.41	3.6	3.43	3.42	3.46	3.41	3.48	3.48
Nd	35.00	38.20	46.2	25	37.7	40.2	47	24.7	36.7	38	47	23	12.9	14.6	13.3	13.7	13.3	13.4	13.1	13.5
Sm	6.76	6.91	7.84	5.1	7.58	7.75	8.49	5.5	6.63	7.04	7.34	5.14	2.91	3.18	2.81	2.76	2.81	2.79	2.96	2.87

Eu	1.70	1.65	1.84	1.34	1.8	1.79	1.97	1.43	1.64	1.63	1.84	1.34	.83	.87	.76	.78	.75	.8	.81	.85
Gd	6.06	5.66	6.33	4.68	6.24	5.94	6.75	4.94	5.86	5.83	6.18	4.64	2.84	2.92	2.75	2.85	2.83	2.68	2.77	2.79
Tb	.87	.83	.93	.74	.9	.87	.96	.76	.81	.74	.85	.66	.47	.48	.45	.44	.44	.45	.45	.46
Dy	4.62	4.01	4.6	3.94	4.72	4.42	5.16	4.1	4.07	4.4	5.03	3.63	2.78	2.85	2.75	2.63	2.7	2.76	2.87	2.77
Ho	.83	8	.9	.77	.84	.8	.94	.8	.73	.71	.97	.83	.57	.57	.53	.51	.51	.54	.55	.54
Er	2.42	2.14	2.64	2.31	2.28	2.23	2.62	2.29	2.13	2.06	2.36	2.25	1.75	1.79	1.56	1.56	1.5	1.46	1.58	1.55
Tm	.34	.31	.38	.34	.33	.33	.39	.33	.29	.3	.37	.29	.26	.27	.22	.24	.24	.25	.23	.24
Yb	2.11	1.92	2.36	2.02	2	2.11	2.44	2.1	1.8	1.92	2.4	1.91	1.61	1.73	1.54	1.48	1.67	1.56	1.56	1.6
Lu	.31	.31	.37	.31	.29	.3	.37	.32	.26	.28	.38	.29	.26	.27	.25	.26	.22	.25	.26	.26
(La/Yb) _N	11.18	15.73	16.28	7.44	12.00	14.79	16.30	7.58	12.25	15.80	15.31	8.12	6.07	6.00	6.35	6.70	5.73	6.48	6.22	6.36
(La/Lu) _N	11.73	15.01	16.00	7.47	12.75	16.03	16.56	7.66	13.06	16.69	14.90	8.24	5.79	5.92	6.02	5.87	6.70	6.23	5.75	6.03
(Yb) _N	10.10	9.19	11.29	9.67	9.57	10.10	11.67	10.05	8.61	9.19	11.48	9.14	7.70	8.28	7.37	7.08	7.99	7.46	7.46	7.66
Eu/Eu*	.80	.78	.77	.82	.78	.78	.77	.82	.79	.76	.81	.82	.87	.86	.83	.84	.81	.88	.85	.91
CIA	37.10	41.86	42.47	34.60	39.52	42.69	42.53	34.01	38.35	42.11	39.31	32.95	45.42	45.59	46.05	46.06	46.15	46.02	45.96	45.92
WIP	91.90	92.32	97.49	92.60	89.53	94.34	99.07	93.21	90.94	91.94	98.16	93.30	71.54	71.47	70.36	69.67	69.83	69.78	70.89	71.27
Mg#	54	55	48	61	54	56	48	62	54	55	49	60	52	53	51	51	51	51	52	53

Notes: Fe₂O₃^{tot} = total iron as Fe₂O₃, LOI = loss on ignition, Eu/Eu* = (Eu_N)/(1/2(Sm_N + Gd_N)) and Mg# (Mg-number) = 100 × MgO/(MgO + 9Fe₂O₃^{tot}). WIP: Weathering Index of Parker = 100 × [(2Na₂O/.35) + (MgO/.9) + (2K₂O/.25) + (CaO/.7)]; 1970); CIA: Chemical Index of Alteration = 100 × molar [(Al₂O₃ + CaO + Na₂O + K₂O)] (Nesbitt & Young, 1982).

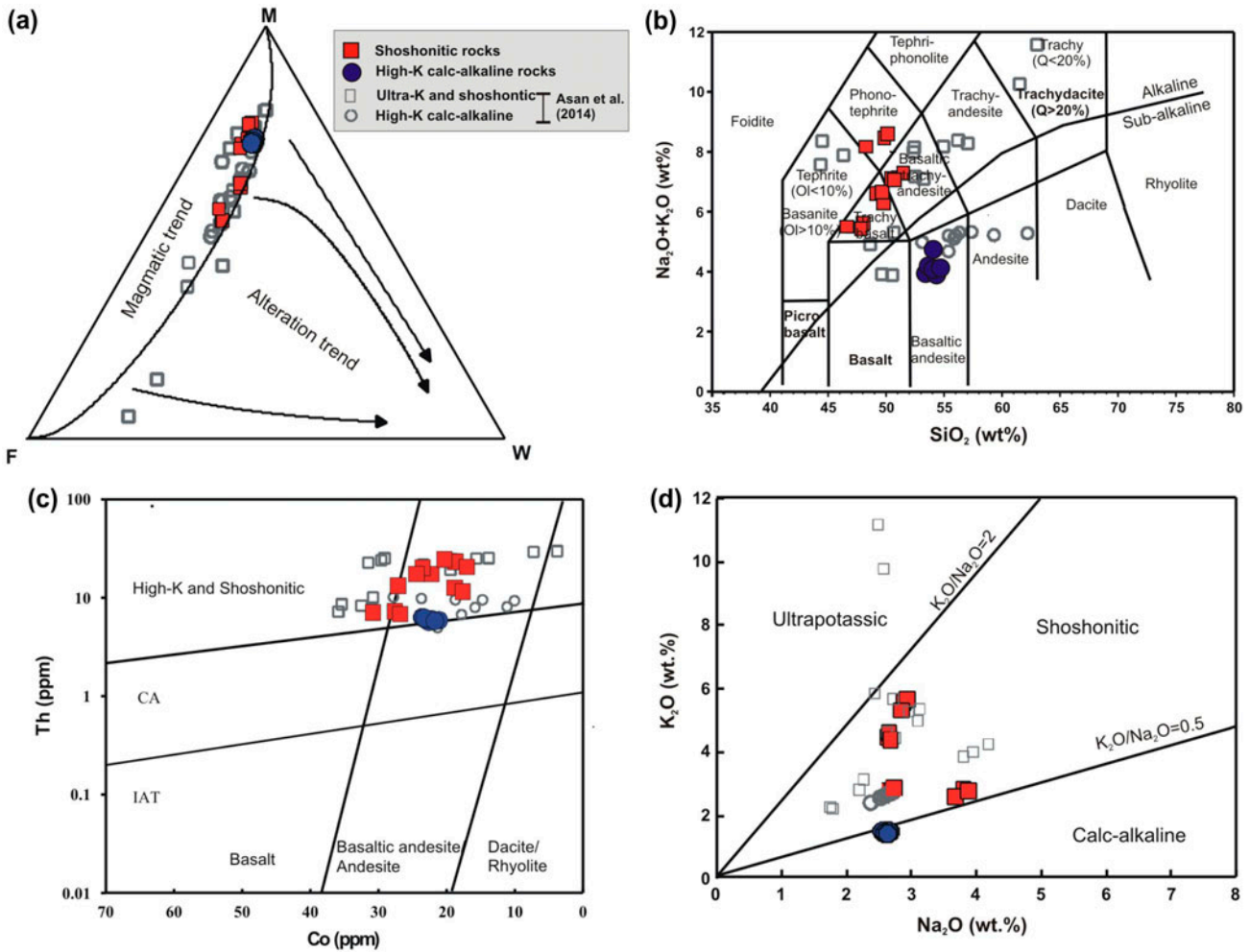


Figure 7. Whole-rock classification and discrimination plots of the Hamsilos volcanic rocks. (a) MFW ternary plot of Ohta and Arai (2007), (b) $\text{Na}_2\text{O} + \text{K}_2\text{O}$ wt% vs. SiO_2 wt% diagram (Le Bas et al., 1986), the division between the alkaline and sub-alkaline fields defined by Irvine and Baragar (1971), (c) Th (ppm) vs. Co (ppm) (Hastie et al., 2007), (d) K_2O vs. Na_2O (Foley, Venturelli, Green, & Toscani, 1987). The expansion of MFW is $M = -0.395 \times \ln(\text{SiO}_2) + 0.206 \times \ln(\text{TiO}_2) - 0.316 \times \ln(\text{Al}_2\text{O}_3) + 0.160 \times \ln(\text{Fe}_2\text{O}_3) + 0.246 \times \ln(\text{MgO}) + 0.368 \times \ln(\text{CaO}^*) + 0.073 \times \ln(\text{Na}_2\text{O}) - 0.342 \times \ln(\text{K}_2\text{O}) + 2.266$; $F = 0.191 \times \ln(\text{SiO}_2) - 0.397 \times \ln(\text{TiO}_2) + 0.020 \times \ln(\text{Al}_2\text{O}_3) - 0.375 \times \ln(\text{Fe}_2\text{O}_3) - 0.243 \times \ln(\text{MgO}) + 0.079 \times \ln(\text{CaO}^*) + 0.392 \times \ln(\text{Na}_2\text{O}) + 0.333 \times \ln(\text{K}_2\text{O}) - 0.892$; $W = 0.203 \times \ln(\text{SiO}_2) + 0.191 \times \ln(\text{TiO}_2) + 0.296 \times \ln(\text{Al}_2\text{O}_3) + 0.215 \times \ln(\text{Fe}_2\text{O}_3) - 0.002 \times \ln(\text{MgO}) - 0.448 \times \ln(\text{CaO}^*) - 0.464 \times \ln(\text{Na}_2\text{O}) + 0.008 \times \ln(\text{K}_2\text{O}) - 1.374$.

calc-alkaline samples that tend to flatten towards LREE and HREE, come up with the significant effect of clinopyroxene fractionation (Thirlwall et al., 1994) on the evaluation of the studied rocks (Figure 9(c) and (d)). The shoshonitic and high-K calc-alkaline samples display no or slight negative Eu anomalies (mean $\text{Eu}_N/\text{Eu}^* = .76\text{--}82$ and $.81\text{--}91$, respectively) suggesting insignificant plagioclase fractionation or oxygen fugacity (Figure 9(c) and (d)).

4.5.3. Sr–Nd–Pb isotopes

Initial Nd–Sr–Pb isotope ratios and epsilon neodymium values (ϵ_{Nd}) of shoshonitic rocks and high-K calc-alkaline volcanic rocks were calculated using the ages of 78 and 72 Ma, respectively (Tables 6 and 7). $^{87}\text{Sr}/^{86}\text{Sr}_{(i)}$ (.70615–.70796) and $^{143}\text{Nd}/^{144}\text{Nd}_{(i)}$ (.51228–.51249) isotopic ratios (Table 6), are plotting in the enriched mantle quadrant of a Sr–Nd correlation diagram, and indicating

a pronounced negative correlation between Sr and Nd isotopic composition (Figure 10(a)). The high-K calc-alkaline volcanic rocks show I_{Sr} (72 Ma) .70618 and of ϵ_{Nd} (72 Ma) -1.0 . The corresponding Nd model age (T_{DM}) is 1.10 Ga. Shoshonitic volcanics show I_{Sr} (78 Ma) (.70751–.70796) and ϵ_{Nd} (78 Ma) values (-5.0 to -3.5). The corresponding Nd model ages (T_{DM}) range from 1.08 to 1.19 Ga. The Sr–Nd isotopic compositions of the Hamsilos shoshonitic and high-K calc-alkaline rocks are plot close to the field of the central–eastern Pontide potassic rocks (Altherr et al., 2008; Asan et al., 2014; Eyüboğlu, 2010) (Figure 10(a)).

Lead isotopic ratios of high-K calc-alkaline rocks are ($^{206}\text{Pb}/^{204}\text{Pb}$) = 18.75, ($^{207}\text{Pb}/^{204}\text{Pb}$) = 15.64 and ($^{208}\text{Pb}/^{204}\text{Pb}$) = 38.79, which are similar to those of shoshonitic rocks [($^{206}\text{Pb}/^{204}\text{Pb}$) = 18.74–18.80, ($^{207}\text{Pb}/^{204}\text{Pb}$) = 15.65, and ($^{208}\text{Pb}/^{204}\text{Pb}$) = 38.84 to 38.88]. The northern hemisphere reference line was used

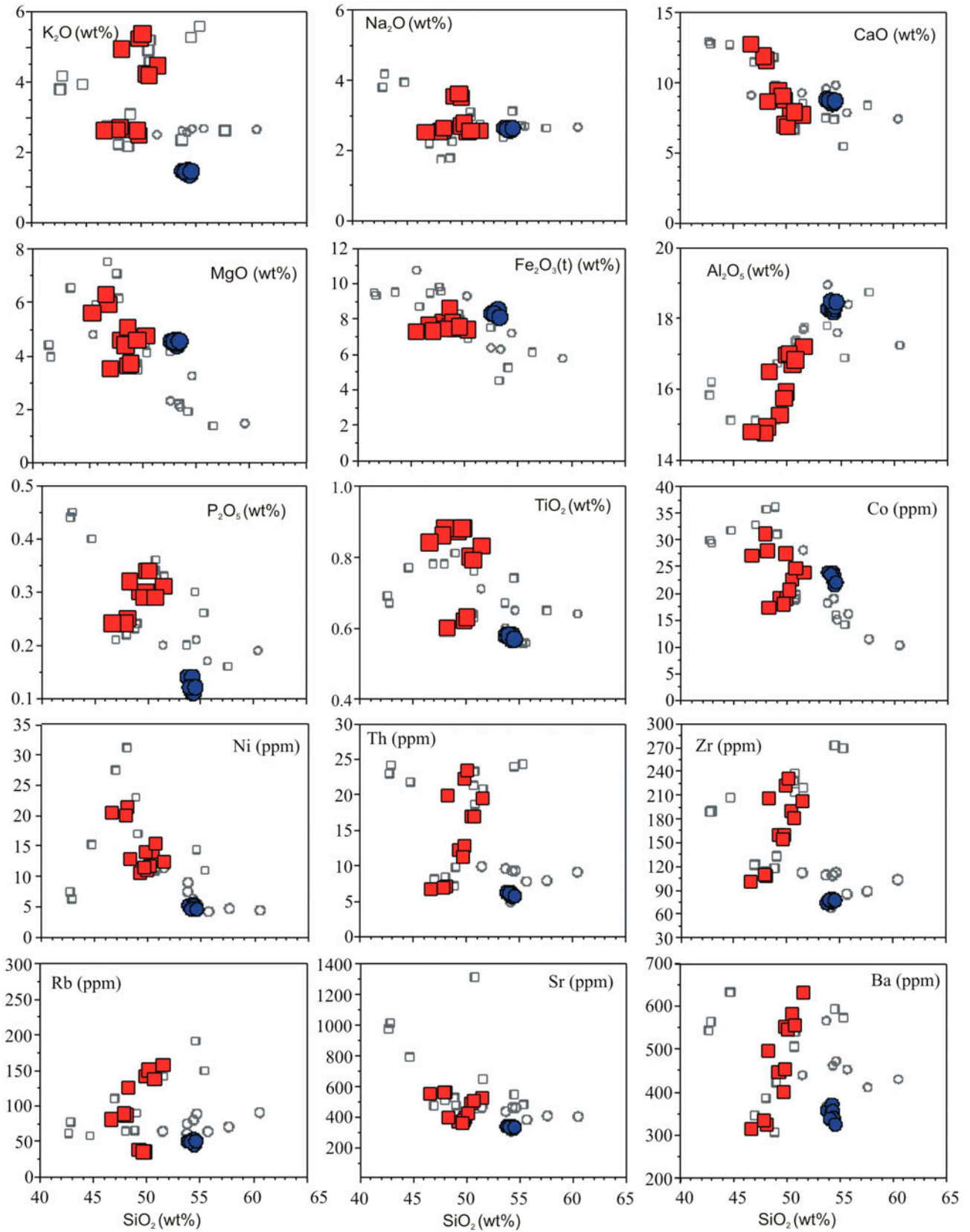


Figure 8. Harker variation diagrams for the studied volcanic rocks (symbols are the same as in Figure 7(a)).

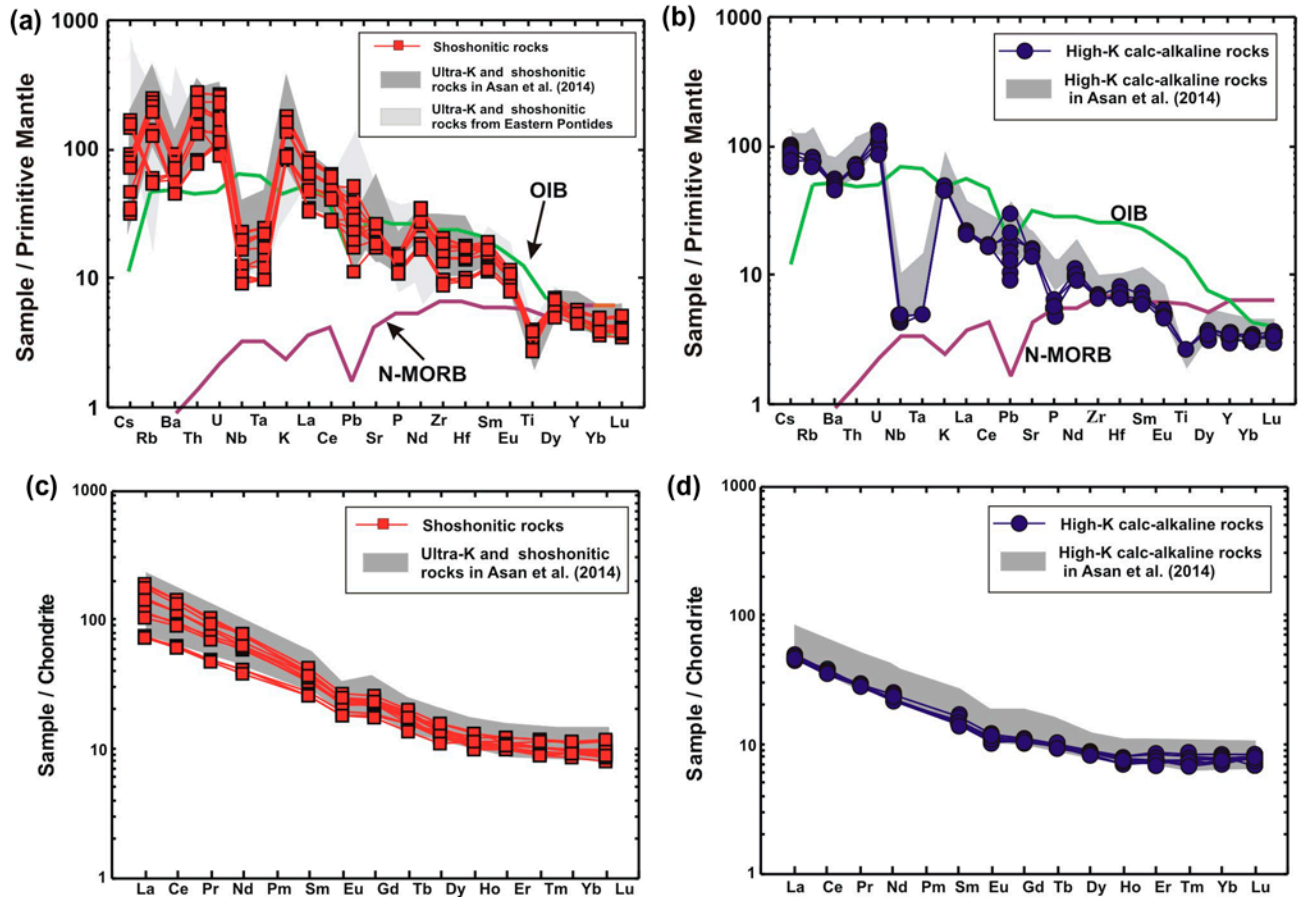


Figure 9. Primitive Mantle-normalized multi-element abundances (a, b) and chondrite-normalized REE patterns (c, d). The PM values are from Sun and McDonough (1989) and chondrite values are from Boynton (1984). Data for the Hamsilos volcanics and Ultra-K and shoshonitic rocks from the Eastern Pontides from Altherr et al. (2008), Eyüboğlu (2010), Asan et al. (2014), Gülmez and Genc (2015), (symbols are the same as in Figure 7(a)).

in the plots because ^{208}Pb data are more radiogenic than ^{206}Pb data. Also plotted for comparison are EM1 (enriched mantle with intermediate $^{87}\text{Sr}/^{86}\text{Sr}$, low $^{143}\text{Nd}/^{144}\text{Nd}$ and low $^{206}\text{Pb}/^{204}\text{Pb}$) and EM2 (enriched mantle with high $^{87}\text{Sr}/^{86}\text{Sr}$, intermediate $^{143}\text{Nd}/^{144}\text{Nd}$, and high $^{206}\text{Pb}/^{204}\text{Pb}$; Zindler & Hart, 1986). All of the samples are highly homogeneous in lead isotopic compositions (Figure 10(b) and (c)) and are plotted between EM1 and EM2 (albeit closer to EM2).

5. Discussion

5.1. Petrogenesis of Hamsilos volcanic rocks

The basic factors that determine the major element, trace element and isotope contents of Hamsilos volcanites include the chemical compositions of the magma source and the petrogenetic processes exposed during magma formation. Geochemical characteristics show that the magma that forms the Hamsilos volcanites was differentiated from a mantle-derived enriched magma. Fractionation and assimilation processes following partial melting seem to have effective role in the formation of final geochemical composition of the studied volcanic rocks. In this section, the importance and function of magmatic

processes in the petrogenesis of the analysed volcanics are discussed and interpreted.

5.1.1. Partial melting

Significant components of arc magmas are derived from mantle wedge (Hochstaedter, Kepezhinskas, Defant, Drummond, & Koloskov, 1996), metasomatised by fluids (from altered oceanic crust or subducted sediments) (Elliott et al., 1997; Smith, Holm, & Thirlwall, 2008; Tatsumi et al., 1986; Turner et al., 1997). Arc magmas result from the partial melting of the metasomatised lithospheric mantle with the effect of the subducted oceanic crust and fluids (Greene, Debari, Kelemen, Blusztajn, & Clift, 2006).

The Hamsilos volcanic rocks possess MgO (Mg# = 48–61) value of 4–6%, Ni value of 5–20 ppm and Cr value of 14–199 ppm. These values indicate that Hamsilos volcanic rocks substantially differ from basaltic rocks that have primitive composition (Mg number > 70, Ni > 200 ppm, Cr > 400 ppm; Green, Schmidt, & Hibberson, 2004). Low Zr/Y and high Zr/Nb ratios (Menzie & Kyle, 1990) generally attributed to a high-level partial melting in subduction-related volcanic arcs. The Hamsilos volcanic rocks have low Zr/Y (5–9) and

Table 6. Whole-rock Sr and Nd isotopic composition for the Hamsilos volcanic rocks.

Sample	Rb (ppm)	Sr (ppm)	⁸⁷ Rb/ ⁸⁶ Sr	⁸⁷ Sr/ ⁸⁶ Sr	2σ	I _{Sr}	Sm (ppm)	Nd (ppm)	¹⁴⁷ Sm/ ¹⁴⁴ Nd	¹⁴³ Nd/ ¹⁴⁴ Nd	(¹⁴³ Nd/ ¹⁴⁴ Nd) _i	2σ	ε _{Nd} (0)	ε _{Nd}	T _{DM} [*] (Ga)
<i>Shoshonitic (78 Ma)</i>															
S-1	38.0	371.0	.30	.70784	13	.70751	6.76	35.00	.1173	.51236	.512300	6	-5.4	-4.6	1.19
S-3	140.6	393.0	1.03	.70911	10	.70796	7.84	46.20	.1030	.51233	.512280	3	-6.0	-5.0	1.08
S-5	86.5	559.8	.45	.70836	11	.70787	5.10	25.00	.1239	.51242	.512360	7	-4.2	-3.5	1.17
<i>High-K calc-alkaline (72 Ma)</i>															
I-6	49.6	339.3	.42	.70662	11	.70618	2.91	12.90	.1370	.51256	.512490	6	-1.0	-1.0	1.10

Notes: ε_{Nd} = ((¹⁴³Nd/¹⁴⁴Nd)_{sample} / (¹⁴³Nd/¹⁴⁴Nd)_{CHUR} - 1) × 10,000, (¹⁴³Nd/¹⁴⁴Nd)_{CHUR} = .512638 (Jacobsen & Wasserburg, 1980). Nd single-stage model ages (T_{DM}^{*}) are calculated with a depleted-mantle reservoir and present-day values of ¹⁴³Nd/¹⁴⁴Nd = .513151 and ¹⁴⁷Sm/¹⁴⁴Sm = .219 (Liew & Hofmann, 1988).

Table 7. Whole-rock lead isotopic composition for the Hamsilos volcanic rocks.

Sample no.	Pb (ppm)	$^{206}\text{Pb}/^{204}\text{Pb}$	$(^{206}\text{Pb}/^{204}\text{Pb})_i$	$^{207}\text{Pb}/^{204}\text{Pb}$	$(^{207}\text{Pb}/^{204}\text{Pb})_i$	$^{208}\text{Pb}/^{204}\text{Pb}$	$(^{208}\text{Pb}/^{204}\text{Pb})_i$
<i>Shoshonitic</i>							
S-1	4.90	18.743	18.313	15.649	15.629	38.849	38.206
S-3	5.50	18.796	18.001	15.652	15.614	38.883	37.839
S-5	4.40	18.793	18.349	15.650	15.629	38.841	38.427
<i>High-K calc-alkaline</i>							
I-6	3.50	18.75	18.167	15.639	15.611	38.785	38.361

medium-level Zr/Nb (14–27) ratios (Figure 11(a)), indicating that the parental magma of the analysed volcanites was originated from a mantle source by low partial melting. Degree of partial melting rate in volcanic arc settings generally depends on the thickness of the subducted crust and varies from 2 to 25% (Plank & Langmuir, 1998).

In magmatic systems, La/Sm ratio is a significant parameter that is controlled by partial melting as well. Meanwhile, low La/Sm ratio points a high degree of partial melting and the presence of remnant spinel, whereas high La/Sm ratio indicates a low degree of partial melting and a garnet remnant balance. Therefore, relatively low La/Sm and partially depleted HREE contents of the studied rocks may have resulted from relatively high-level partial melting of the source, namely a mantle rock that contains spinel. The REE models developed using fractional and batch partial melting equations of Shaw (1970) suggest that Hamsilos volcanics originated from a mantle material with the spinel–peridotite composition through 1–3% partial melting (Figure 11(b)).

The shoshonitic volcanic rocks are characterised by the enrichment of large ion lithophile elements and LREEs compared with the high-K calc-alkaline volcanic rocks, and these differences in source characterisation indicate a low degree of partial melting for the shoshonitic volcanic rocks. The shoshonitic melts in the Hamsilos volcanic rocks can be derived from a low degree of partial melting of an enriched SCLM, while the high-K calc-alkaline melts can be derived from relatively high degree of partial melting of an enriched SCLM source (Figure 9(c) and (d)).

5.1.2. Fractional crystallisation and assimilation vs. magma mixing

Hamsilos volcanic rocks possess low MgO, Ni and Co contents. Major and trace element variation diagrams show that fractionation from a more basic magma has been playing affective role in the development of volcanites (Figures 8 and 9). The eventual decrease in the TiO_2 and Fe_2O_3^* contents as opposed to the increase in the SiO_2 content of Hamsilos volcanic rocks indicates the fractionation of Fe–Ti oxides; meanwhile, the negative relations in SiO_2 vs. CaO, Fe_2O_3^* and MgO reveal the fractionation of plagioclase ($\text{An} > 50$) and clinopyroxene phases from the parental magma. The presence of a relatively negative anomaly in Eu values of the rocks in the

chondrite-normalised REE distributions of the analysed volcanic rocks indicates that plagioclase fractionation is influential in rock development (Figure 9(c) and (d)).

There is not a clear fractional crystallisation trend in Figure 12(a) and (b) for high-K calc alkaline rocks. All the high-K calc-alkaline rocks are clustered within the narrow range but in Figure 12(a) and (b), negative variations between Zr vs. Co and Ni indicate the function of crystal fractionation in the development of the shoshonitic rocks in the Hamsilos volcanic rocks. The decreasing $\text{CaO}/\text{Al}_2\text{O}_3$ ratio against increasing $\text{Fe}_2\text{O}_3^*/\text{MgO}$ ratio of Hamsilos volcanites imply that clinopyroxene fractionation from the parental magma exerts a certain influence (Figure 12(c)). Moreover, increasing Al_2O_3 against decreasing $\text{CaO}/\text{Na}_2\text{O}$ exhibits that clinopyroxene fractionation affects the evolution of volcanic rocks (Figure 12(d)).

The relation between the source metasomatism by fluids from subduction zone and/or crustal assimilation and fractionation can be explained in the diagram where trace element ratios such as Nb/Y vs. Rb/Y are used (Figure 13). Considering this diagram, whereas the high-K calc-alkaline samples indicate subduction zone enrichment trends, the shoshonitic rocks samples show specific subduction zone enrichment or crust contamination trends. This plot also indicates that when the Hamsilos volcanics are generally similar trends of the samples of the previous study by Asan et al. (2014).

$(^{143}\text{Nd}/^{144}\text{Nd})_i$ vs. SiO_2 (wt%) and Zr/Y vs. Zr (ppm) plots reveal the influence of assimilation, rather than fractional crystallisation on the evolution of shoshonitic rocks but not say anything high-K calc-alkaline rocks (Figure 14(a) and (b)). Another important argument is that some of the variation diagrams, such as the element vs. element ratio (Figure 14(c) and (d); Langmuir, Vocke, Hanson, & Hart, 1978), display a linear trend of the studied volcanic rocks, all of which confirm the derivation assimilation and/or magma mixing.

The texture and composition of minerals are related to the different types of disequilibrium that occur during volcanic evolution. The magma mixing processes can be determined by following as (1) petrographic or textural criteria, which contain the disequilibrium of textures such as sieved plagioclases (Dungan & Rhodes, 1978), the reaction rim and resorption in clinopyroxenes, the presence of unsieved and sieved plagioclases in the same sample (Stimac & Pearce, 1992), and the rounded and embayed crystals (Stimac & Pearce,

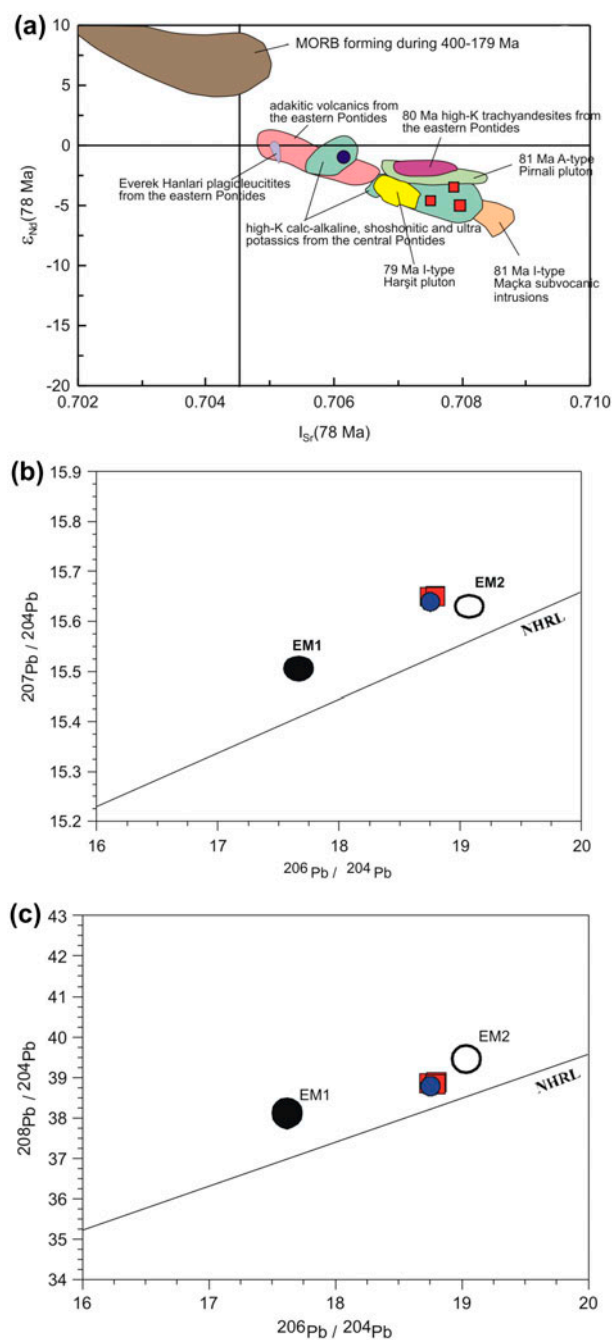


Figure 10. (a) $\epsilon_{Nd}(t)$ vs. $I_{Sr}(t)$ isotope compositions of the Hamsilos volcanic rocks. Symbols are the same as in Figure 6(a). Data sources are as follows: 400–179 Ma MORB is from Mahoney et al. (1998), Xu et al. (2003), Tribuzio, Thirlwall, Vannucci, and Matthew (2004) and Xu and Castillo (2004). Adakitic volcanics from the eastern Pontides (Aydıncakır, 2014; Dokuz et al., 2013; Karsli et al., 2011; Topuz et al., 2005), Eastern Pontide Paleocene plagioclucites (Altherr et al., 2008), Campanian I-type Harşit pluton (Karsli et al., 2010) and Maçka subvolcanic intrusions (Aydın, 2014), Campanian A-type Pirmali rocks (Karsli et al., 2012), Eastern Pontide high-K volcanic rocks (Eyüboğlu, 2010), high-K calc-alkaline, shoshonitic and ultra-potassics from the Central Pontides (Asan et al., 2014), (b) $^{207}\text{Pb}/^{204}\text{Pb}$ vs. $^{206}\text{Pb}/^{204}\text{Pb}$ and (c) $^{208}\text{Pb}/^{204}\text{Pb}$ vs. $^{206}\text{Pb}/^{204}\text{Pb}$ for the selected samples from the Hamsilos volcanic rocks. EM1 and EM2 were taken after Zindler and Hart (1986). NHRL (The Northern Hemisphere Reference Line) after Hart (1984).

1992); (2) compositional criteria, which include the determination of normally and reversely zoned crystals and presence of these crystals in the same sample (Halsort & Rose, 1991; Luhr & Carmichael, 1980). The broad compositional variation, sieved texture and complex zoning of plagioclase are commonly observed in subduction-related basaltic and andesitic rocks, which may refer the presence of highly dynamic magmatic systems (Tepley, Davidson, Tilling, & Arth, 2000). The Hamsilos volcanic rocks include the sieved textured, rounded and embayed plagioclases (Figure 3(b) and (f)). Sieve texture in plagioclases occurs because of magma mixing processes (Tsuchiyama, 1985) or forms because of decompression while rises to a shallower depth (Nelson & Montana, 1992).

The clinopyroxenes in the Hamsilos volcanic rocks (high-K calc-alkaline and shoshonitic rocks) show different types of disequilibrium textures, as zoning, resorbed, rounded crystals and embayed and breakdown clinopyroxenes megacryst (Figures 3 and 4). Clinopyroxenes are represented by rounded and embayed crystals similar to sieved plagioclase crystals that are generally caused by magma mixing (Hibbard, 1981; Simonetti Shore, Bell, 1996; Streck, 2008) or decompressional melting (Nelson & Montana, 1992). Normally zoned clinopyroxenes in the Hamsilos volcanic rocks represent more Mg-rich composition in the core compared to the rim coupled with higher Cr and lower Ti and Al contents (Figure 15(a) and (b)). Reverse zoning exhibits the opposite case. In addition, the normally and reversely zoned clinopyroxenes are present both in the shoshonitic and high-K calc-alkaline rocks, suggesting the presence of mixing processes.

5.1.3. Source characteristics

Hamsilos volcanics exhibit the characteristics of typical subduction zone volcanic rocks with depletion of HFSEs (e.g. Nb, Zr, and Ta), enrichment (Figure 9(a) and (b)) of LILEs (e.g. Sr, K, Rb and Ba) and high ratio of Ba/La. These characteristics are present in previously analysed trace element variation diagrams (Baier, Audétat, & Keppler, 2008; Pearce, 1983). Subduction-related continental arc magmas are characterised by LILE enrichment against HFSE, LREE against HREE and negative Nb, Ta, Zr, Hf and Ti anomalies (Hawkesworth, Turner, McDermott, Peate, & Van Calsteren, 1997; Pearce, 1983). Ocean island basalts (OIB) differ from subduction zone continental arc volcanites in terms of the presence of positive Nb, Ta and Ti anomalies (Figure 9(a) and (b)) (Hofmann, 1997). However, slight enrichment in LILE and decrease in negative Nb, Ta and Ti anomalies can be interpreted to the some contribution of asthenospheric melts (OIB), compared to typical of subduction-related magma (Figure 9(a) and (b)). The LILE and LREE enrichment of volcanic rocks (Figure 9) indicates that parental magma can derive from a source area (probably lithospheric mantle) that is enriched (exposed

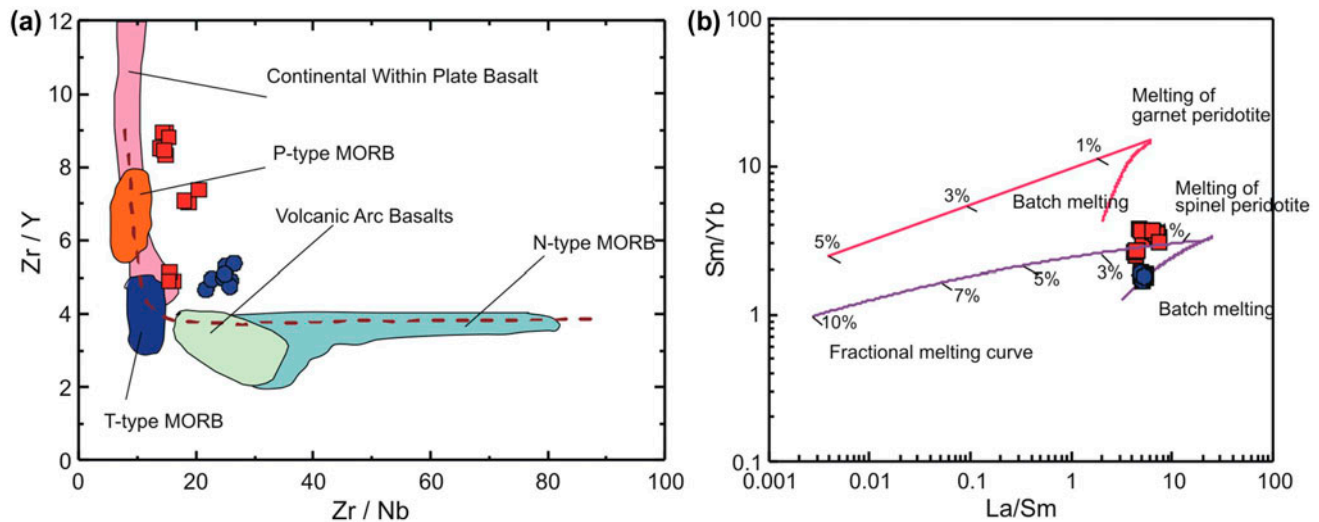


Figure 11. (a) Zr/Y vs. Zr/Nb plot (Menzies & Kyle, 1990) as a measure of amount of partial melting involved in the genesis of the Hamsilos volcanites. The fields of N-, T-, P-type MORBs are taken from Le Roex (1987), (b) La/Sm vs. Sm/Yb diagram showing the melting curves of the samples from the Hamsilos volcanic rocks. Fractional and batch melting equations of Shaw (1970) were used to construct the melting model. Modal mineralogy for the spinel- and garnet-peridotites are taken from Wilson (1989), and $ol_{.66} + opx_{.24} + cpx_{.08} + sp_{.02}$ and $ol_{.63} + opx_{.30} + cpx_{.02} + gt_{.05}$, respectively (ol: olivine, opx: orthopyroxene, cpx: clinopyroxene, sp: spinel, gt: garnet). Trace element composition of the spinel-peridotite (C_0 values) is from McDonough (1990), while that of garnet peridotite is from Frey (1980). K_d s between the basaltic melts and minerals given in the inset are compiled from Irving and Frey (1978), Fujimaki, Tatsumoto, and Aoki (1984), McKenzie and O'Nions (1991) and Rollinson (1993) (symbols are the same as in Figure 7(a)).

to metasomatism) by fluids emerging from the subducted slab and/or sediments (Münker, Wörner, Yogodzinski, & Churikova, 2004). In chondrite-normalised REE diagrams, the HREE values of Hamsilos volcanites exhibit an almost-horizontal trend. This horizontal trend of HREE values suggests that the parental magma that forms Hamsilos volcanic rocks may originate from a spinel lherzolitic (<50 km depth) mantle source, rather than a lherzolitic mantle source that contains garnet (Figure 10(c) and (d)).

Low Sr/Th ratio and moderately radiogenic $^{87}\text{Sr}/^{86}\text{Sr}$ values (.70662–.70911) (Figure 16(a)) indicate that the mantle source was contaminated by fluids or melts derived from subducted sediments. On the basis of $^{87}\text{Sr}/^{86}\text{Sr}$ vs. Sr/Th relationships in a number of arcs, Hawkesworth et al. (1997) noted that high Sr/Th ratios are developed in rocks with low $^{87}\text{Sr}/^{86}\text{Sr}$ (~.704). The rationale for using this plot is that as a result of the preferential mobilisation of the LILE into hydrous fluids, high Sr/Th ratios will be a signature of the fluid phase. The Sr isotope ratios might be expected to be variable, depending on whether the fluids have interacted mainly with altered basaltic crust ($\geq .7047$; Bickle & Teagle, 1992; Staudigel, Davies, Hart, Marchant, & Smith, 1995) or subducted sediment ($> .709$). Thus, these researchers asserted that low $^{87}\text{Sr}/^{86}\text{Sr}$ value supports the addition of fluid component, whereas the high $^{87}\text{Sr}/^{86}\text{Sr}$ values point out the contribution of sediment component. The $^{87}\text{Sr}/^{86}\text{Sr}$ vs. Sr/Th diagrams of rocks in depleted and enriched arcs present a hyperbolic trend (Figure 16(a)). The Hamsilos volcanic rocks together with their low Sr/

Th (<55) ratios and high $^{87}\text{Sr}/^{86}\text{Sr}$ (>.709) values resemble those rocks formed in enriched arcs (Macdonald, Hawkesworth, & Heath, 2000). The role of fluid and melt components in subduction zones can be evaluated using a combination of geochemical parameters. Ba is selectively enriched in fluids because of its higher mobility relative to La, while Th displays preferential enrichment in sediment-derived melts (Kirchenbaur, Munker, Schuth, Garbe-Schonberg, & Marchev, 2012).

The Ba/La vs. Th/Yb diagram is used to show the fluid or sediment inputs in subduction zones (Figure 16(b)). The vertical trend in the diagram indicates the enriched mantle that was metasomatised by subduction fluids, whereas the horizontal trend signifies the enriched mantle source that was metasomatised by subducted sediments. In the diagram, the high-K calc-alkaline rocks are gathered somewhere near the starting point of vertical line indicating the subducted fluid phase (vertical) input, whereas the subducted sediment (horizontal) input is observed for the samples of shoshonitic rocks of the Hamsilos volcanites.

The Ta/Yb vs. Th/Yb diagram (Pearce, 1983) in Figure 16(c) has been used for the discrimination of the mantle sources and the determination of possible additional components such as a subduction and/or crustal contamination of the mantle (Figure 16(c)). All the Hamsilos volcanic rocks have high Th/Yb ratios relative to the mantle array. According to this diagram, while the high-K calc-alkaline rock patterns present subduction enrichment, the shoshonitic rock patterns show the addition of a subducted component to the mantle and

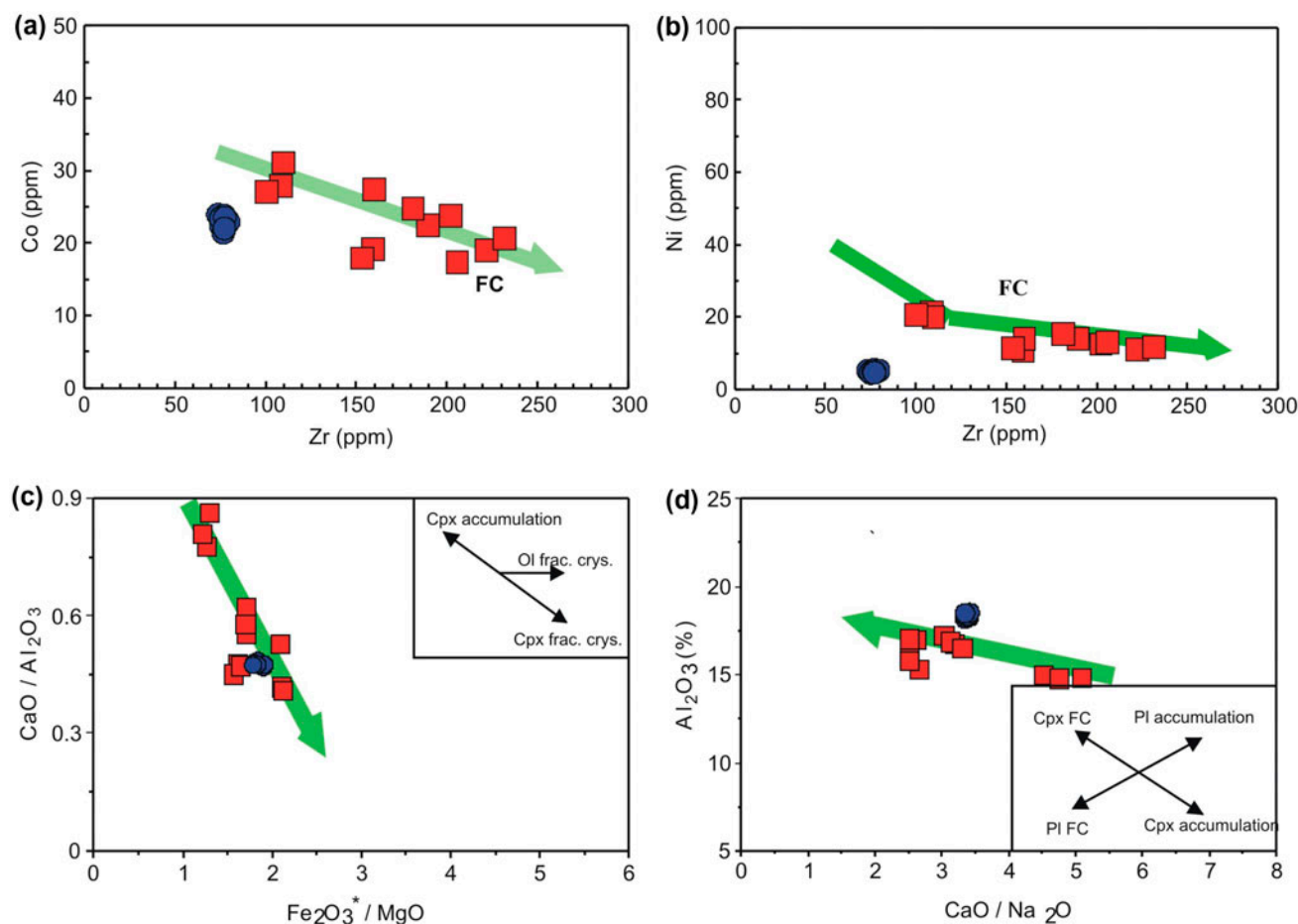


Figure 12. (a) Zr (ppm) vs. Co (ppm), (b) Zr (ppm) vs. Ni (ppm), (c) $\text{Fe}_2\text{O}_3^*/\text{MgO}$ vs. $\text{CaO}/\text{Al}_2\text{O}_3$, (d) $\text{CaO}/\text{Na}_2\text{O}$ vs. Al_2O_3 (wt%) diagrams showing possible fractional crystallisation trends (FC) for the Hamsilos volcanic rocks (symbols are the same as in Figure 7(a)).

contamination from the crust (upper crust). Moreover, the similar interpretations are also supported by data obtained from the study held by Asan et al. (2014). The combined data show that the calc-alkaline and shoshonitic rocks were derived from same mantle source with different degrees of partial melting.

In Figure 16(d), Bradshaw and Smith (1994) and Smith, Sánchez, Walker, and Wang (1999) implied that because HFSE (such as Nb and Ta) are depleted in the lithospheric mantle relative to the LREE, high Nb/La ratios (~ 1) indicate an OIB-like asthenospheric mantle source for basaltic magmas, and lower ratios (~ 0.5) indicate a lithospheric mantle source. Similar to arc volcanites, Hamsilos volcanic rocks possess higher La/Nb (3–5) and Ba/Nb (34–124) ratios than MORB, OIB and continental volcanites (Sun & McDonough, 1989). Considering that HFSEs (e.g. Nb and Ta) are depleted in the lithospheric mantle relative to LREEs, the Nb/La (.20–.30) and La/Yb (9–25) ratios of Hamsilos volcanic rocks suggest a lithospheric mantle source (Figure 16(d)). Average Nb/Ta ratios of 11–12 and ~ 17 indicate the presence of crust-derived magma and mantle-derived magma, respectively (Green, 1995). The Nb/Ta ratios of Hamsilos volcanic rocks vary between 14 and 19. These

values support the derivation of the parental magma of the volcanites from the mantle. In addition, the Zr/Sm ratios of the volcanic rocks range between 20 and 29. Meanwhile, the Zr/Sm values are lower than those in chondrites (~ 25); in N-MORB, E-MORB and OIB (~ 28); in the lower crust (24); in the middle crust (32) and in the upper crust (41). This enriched mantle is metasomatised by subduction components and resembles the source of island arc rocks (Wilson, 1989). This result proves that Hamsilos volcanites are derived from a metasomatised-enriched lithospheric mantle at spinel stability field.

The production of high-K and calc-alkaline associations can be supported by two different theory; (i) the calc-alkaline and high-K magmas were derived from a different lithospheric mantle source at variable levels and enriched by metasomatic events in different degree, (ii) the magmas in these different affinities can be generated from same magma source at same level effected by metasomatic events resulted in heterogeneous source composition (Conticelli, Avanzinelli, Marchionni, Tomasini, & Melluso, 2011). Foley (1992) suggest that co-occurrence of potassic and calc-alkaline magmas can be evolved from progressive melting of veined upper

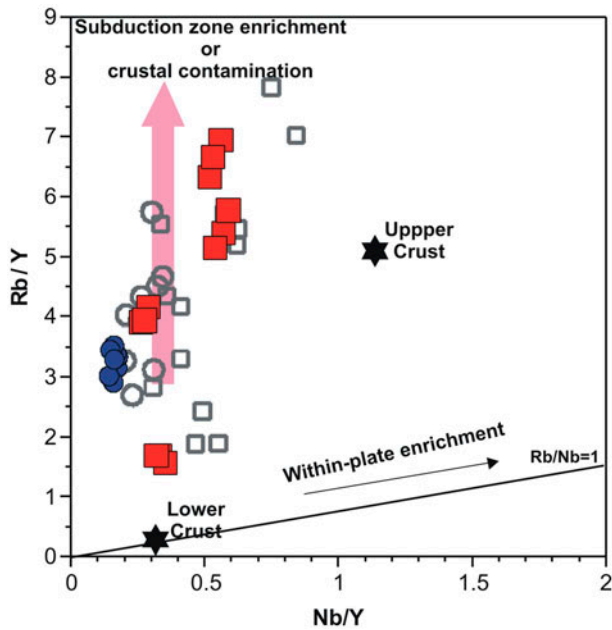


Figure 13. Nb/Y vs. Rb/Y plots of the Hamsilos volcanics (diagram are taken from Pearce et al., 1990; compositions of the upper and lower crusts after Taylor & McLennan, 1985) (symbols are the same as in Figure 7(a)).

mantle source. The production of two mafic end members by a two-stage partial melting processes was suggested by Maria and Luhr (2008) that the high-K magmas are generated mostly from net-veined metasomatic agents, while the magmas in calc-alkaline affinity can be evolved from surrounding lithospheric mantle.

The previous study performed by Asan et al. (2014) in same area suggests that the shoshonitic and ultra-K rocks were derived from metasomatic veins related to melting of recycled subducted sediment, but high-K calc-alkaline rocks from lithospheric source metasomatized by fluids from subduction zone. The enriched LILE, LREE values and more radiogenic $^{87}\text{Sr}/^{86}\text{Sr}$ ratios observed in shoshonitic volcanic rocks in this study can be interpreted that the melts can be derive from a low degree partial melting of an enriched SCLM in heterogeneous composition, while the high-K calc-alkaline melts can be derive from relatively high degree partial melting of the same enriched lithospheric mantle source.

5.2. Geodynamic implications and magma chamber processes

The Pontides orogenic belt has been considered to be an example of well-preserved continental magmatic arcs

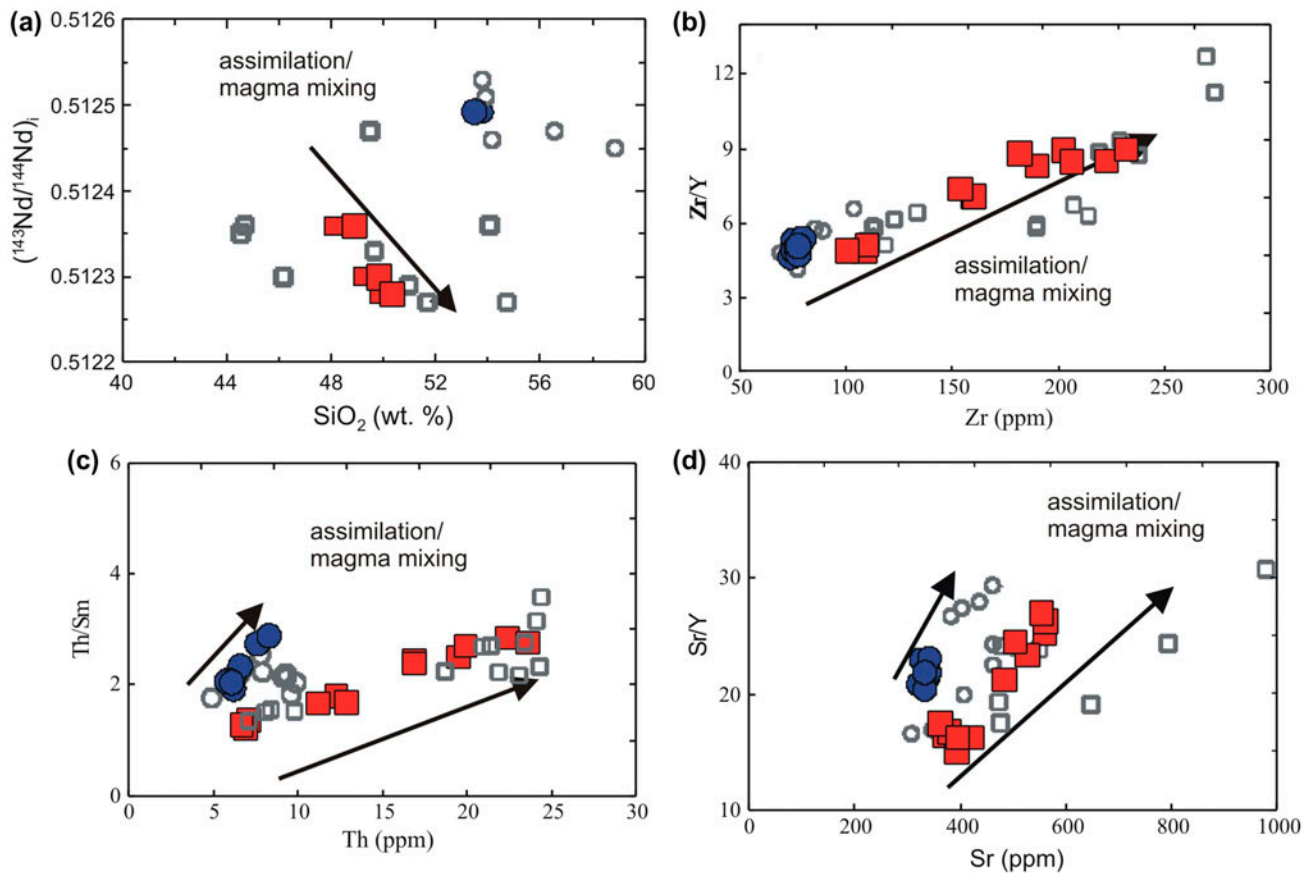


Figure 14. (a) $(^{143}\text{Nd}/^{144}\text{Nd})_i$ vs. SiO_2 (wt%), (b) Zr/Y vs. Zr (ppm), (c) Th/Sm vs. Th (ppm) and (d) Sr/Y vs. Sr (ppm) plots of the shoshonitic and high-K calc-alkaline samples from the Late Cretaceous Hamsilos volcanic rocks (symbols are the same as in Figure 7(a)).

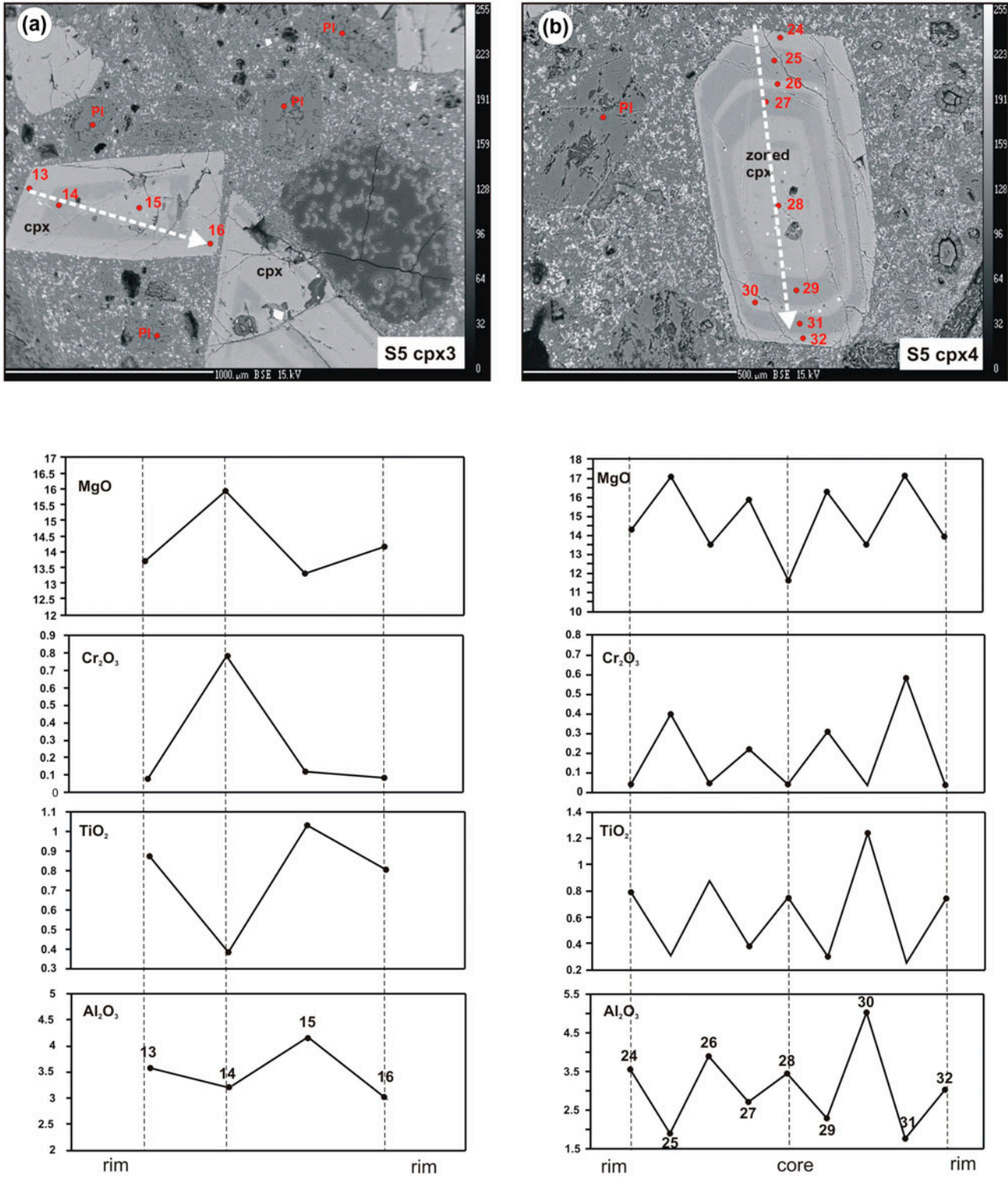


Figure 15. Back-scattered electron images and core to rim compositional variation plots of clinopyroxenes (a, b) from shoshonitic volcanic rocks.

(Aydin, 2014; Aydınçakır, 2014; Karsli et al., 2012; Şengör & Yılmaz, 1981; Yücel, Arslan, Temizel, & Abdioğlu, 2014). This tectonic unit comprises a mountain chain, which is 200 km in wide and extending along the southern Black Sea coast for 500 km. This unit occurs within the Alpine metallogenic system. Through

the late Cretaceous period, the Sakarya Zone experienced intensive magmatic activity associated with subduction (Aydin, 2014; Eyüboğlu, 2010; Genç et al., 2014 et al., 2010; Karsli et al., 2012; Kaygusuz & Aydınçakır, 2009, 2011; Varol, 2013). However, the subduction polarity and geotectonic evolution of the eastern Pontides are

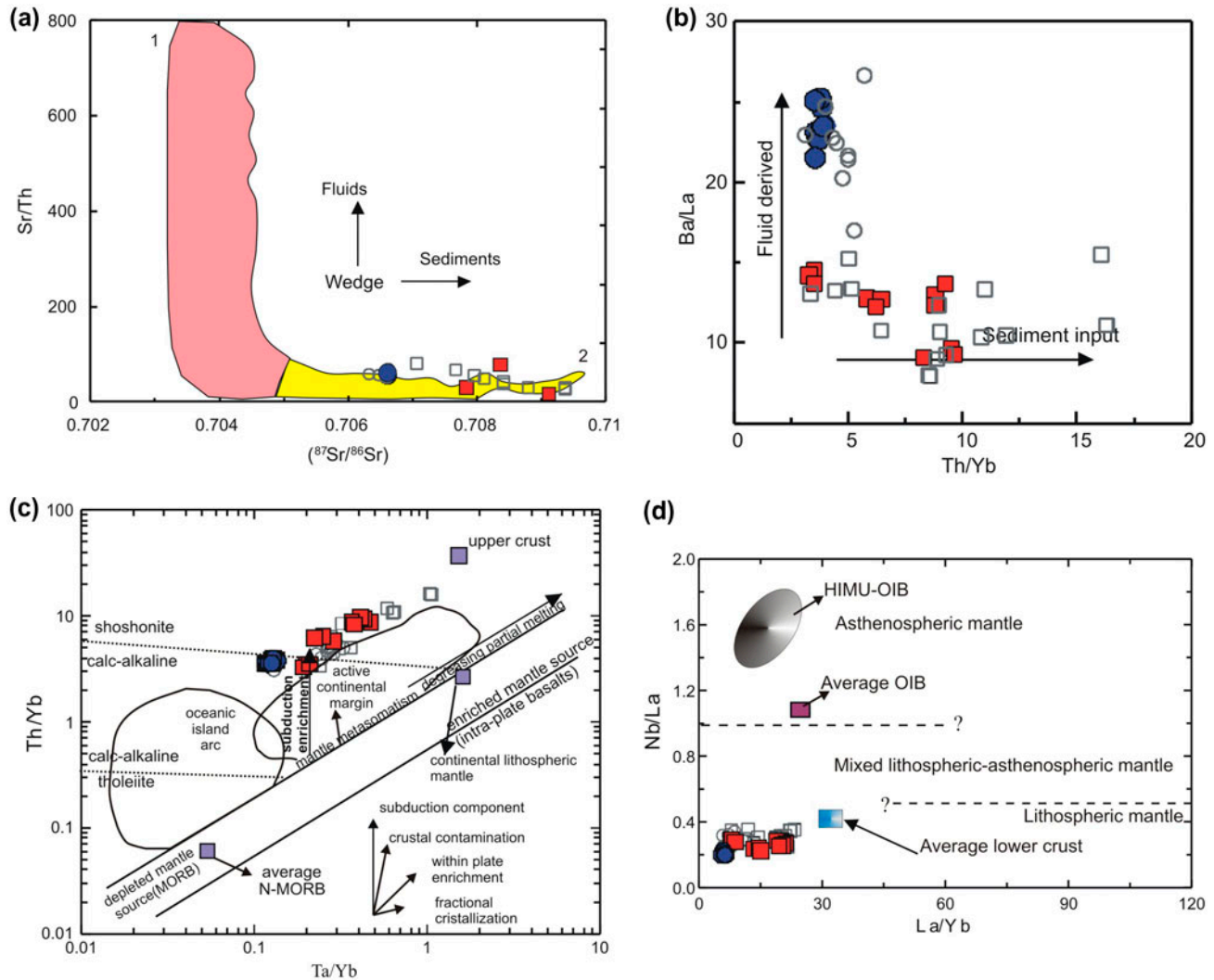


Figure 16. (a) $^{87}\text{Sr}/^{86}\text{Sr}$ vs. Sr/Th variations in Hamsilos volcanic rocks. Fields 1 and 2 enclose data from arcs considered incompatible element depleted and enriched, respectively, by Hawkesworth et al. (1997). The arrows show the sense of enrichment predicted from addition of fluid and sedimentary components to the mantle wedge, (b) Th/Yb vs. Ba/La diagram is from Woodhead, Hergt, Davidson, & Eggins, (1991), (c) Th/Yb vs. Ta/Yb diagram (after Pearce, 1983). Shoshonitic and high-K calc-alkaline rocks of Hamsilos volcanites are characterised by high Th/Yb relative to Ta/Yb ratios and closely resemble those of a mantle source modified by subduction, metasomatism and crustal contamination. Average N-MORB composition and average Continental Crust (Av. CC) are from Sun and McDonough (1989) and Taylor and McLennan (1985), respectively. Vectors show inferred effects of fractional crystallisation (FC), assimilation-fractional crystallisation (AFC), subduction enrichment and mantle metasomatism are from Pearce et al. (1990), (d) The Nb/La vs. La/Yb variation diagram. Average OIB is taken from Fitton, James, & Leeman, (1991) and average lower crust is after Chen and Arculus (1995). Dashed lines separating fields of the asthenospheric, lithospheric and mixed mantle, and the HIMU-OIB field are after Smith et al. (1999) and Weaver, Wood, Tarney, and Joron (1987), respectively (symbols are the same as in Figure 7(a)).

controversial for the Cretaceous period. Several researchers suggested that the eastern Pontides was a magmatic arc that occurred as a result of northward subduction of the Neotethys along the southern border of the Sakarya Zone (Altherr et al., 2008; Karlı et al., 2010; Okay & Şahintürk, 1997; Şengör & Yılmaz, 1981; Şengör et al., 2003; Ustaomer & Robertson, 2010; Yılmaz et al., 1997). Conversely, Dewey et al. (1973), Bektaş et al. (1999), Eyuboglu, Chung, et al. (2011), and Eyuboglu, Santosh, et al. (2011) proposed a southward subduction that continued uninterrupted from the Paleozoic period until the end of the Eocene period. In the light of our

finding and results, we can propose that the Hamsilos lavas were possibly generated in a subduction zone at around 78 Ma in the Sakarya Zone.

The Hamsilos volcanic rocks exhibit the characteristics of subduction zone volcanic rocks with depletion of HFSEs (e.g. Nb, Zr, and Ta), enrichment (Figure 9(a) and (b)) of LILEs (e.g. Sr, K, Rb, and Ba) and high ratio of Ba/La. These characteristics are shown in the trace element variation diagrams (Figure 9(a) and (b)). The Hamsilos volcanics have geochemical characteristics typical for those of subduction-related arc magmas, characterised by LILE enrichment relative to HFSE and LREE

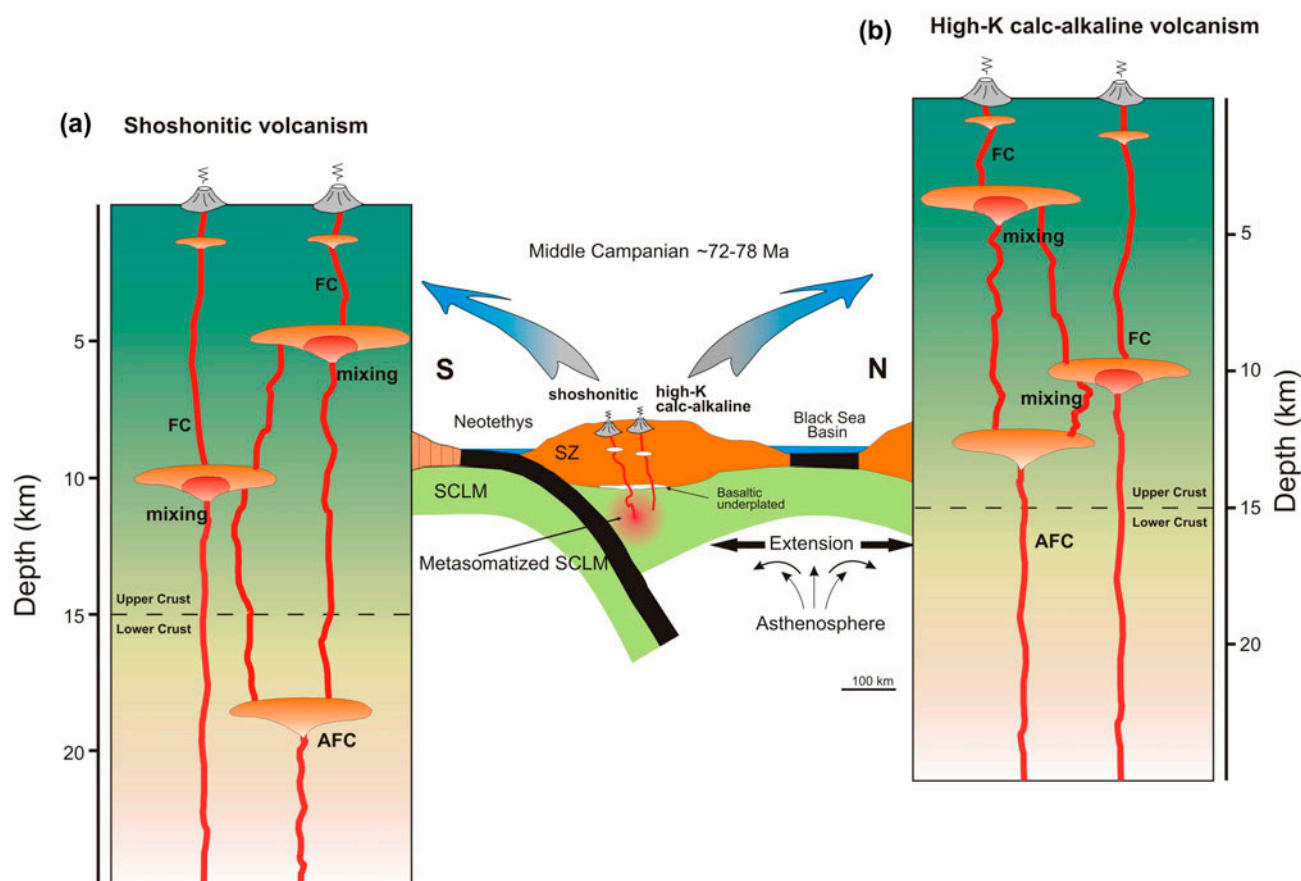


Figure 17. Schematic cross section of the Late Mesozoic geodynamic evolution of the central part of the Sakarya Zone in the late Santonian to Campanian (at 85–70 Ma). (a, b) pre-eruptive crystallisation paths and magmatic processes in crustal magma chambers (SCLM: Subcontinental Lithospheric Mantle).

enrichment relative to HREE, and negative Nb, Ta, Zr, Hf and Ti anomalies (Hawkesworth et al., 1997; Pearce, 1983). However, OIB-like features such as high-K nature, LILE enrichment and weak negative Ta, Nb and Ti anomalies indicate some melt addition from undepleted mantle source. In addition, samples of Hamsilos volcanic rocks present Sr–Nd isotopic characteristics that are markedly similar to shoshonitic trachyandesites (80 Ma), which were interpreted as mantle-derived rocks by Eyüboğlu (2010) and Gülmez and Genc (2015) that formed at an extensional environment of subduction setting (Figure 10(a)).

On the basis of the above discussion, a simplified cartoon can be used to illustrate relationships between the petrogenesis and tectonic environment of Hamsilos volcanics. I recommend that the Hamsilos volcanics formed in an extensional environment above subduction zone. During the middle Campanian (~78 Ma), fore arc/inter-arc region of the Sakarya Zone was underwent an extensional regime, as evidenced by the high-K nature of basic volcanic rocks (Altherr et al., 2008; Asan et al., 2014; Aydin, 2014; Eyüboğlu, 2010; Gülmez & Genc, 2015).

According to geochemical evidence, the parent magma of the Hamsilos volcanic rocks has been interpreted as generated in a sub-continental lithospheric mantle source that enriched by fluids and/or sediments from a subduction of oceanic crust. The enriched magmas composing the shoshonitic and high-K calc-alkaline volcanic rocks have polybaric evolutionary mechanism during the magma transportation at crustal levels. The fracturing of the crust because of extension in back-arc setting can provide appropriate pathway for rising magma. These magmas are stalled at different crustal levels and can be explained by different petrological processes such as FC, AFC and magma mixing to modify the observed disequilibrium of the textural, petrographical and mineral chemical features of the Hamsilos volcanic rocks.

The clinopyroxene thermobarometric calculation combined with the petrographic and mineral chemistry data reveal that the two different magma storage levels were specified for shoshonitic volcanic rocks (Figure 17(a)). The clinopyroxene barometer were yielded pressures between 1.8 and 6.2 kbar, thus indicating early crystallisation processes at deep to mid-crustal level

(~18 km). The crystallisation of olivine and clinopyroxene with high Mg number was present at this level and they were accompanied by the crystallisation of high-Ca plagioclases. The presence of clinopyroxenes having Mg- and Cr-rich mantle composition (Figure 15(a) and (b)) than their core and rim can be accepted as evidence for replenishment of this magma chambers by relatively mafic and hot magma. Moreover, the assimilation of host lower crust may take place at this level. The mentioned magmas were risen and ponded at shallow crustal level. These magma chambers were characterised by the presence of phlogopite and relatively low-Ca plagioclase, clinopyroxenes. The data obtained from biotite thermometer indicate that the magma reservoir take place around 5 km in depth. The occurrence of disequilibrium textures as zoned, resorbed and embayed clinopyroxenes and sieved, embayed and rounded plagioclases (Figure 4(a)–(e)) was arise from petrological processes as magma mixing, as well as decompression. The presence of normally and reversely zone clinopyroxene in same sample can support the idea of the mixing processes. The magmas rises again and ponded pre-eruptive shallow level magma chambers. The crystallisation of low-Ca plagioclases and analcimes (replacement of leucite) happened at this level. All of the textural and thermobarometric parameters can be interpreted as open-system behaviours during crystallization as indicated by Yücel, Arslan, et al. (2014).

The crystallisation history of high-K calc-alkaline volcanic rocks has similarities with the shoshonitic volcanic rocks (Figure 17(b)). The only-clinopyroxene thermometer yielded the crystallisation pressure are between 1.5 and 3.6 kbar corresponding ~5–12 km crystallisation depth. The crystallisation of clinopyroxene, plagioclases and olivine started at mid crustal magma chambers approximately 12 km in depth. The magmas raise and stalled at higher level magma chamber. At this level, the magma chamber is replenished by orthopyroxene bearing relatively more primitive magmas and the mixing processes took place. The mixing of fractionated and primitive magmas leads to the occurrence of reversely zoned clinopyroxenes and plagioclases. The magma rises again and ponded at shallow level crustal magma chamber and underwent the processes of FC and mixing. These magma chambers are characterised by crystallisation of fractionated phases as sieved-textured plagioclases with low anorthite content, sanidine and clinopyroxene microlites with relatively low Mg number.

6. Conclusions

This study provides new constraints for the geodynamic evolution of the Central Pontides. The results are as follows:

- (1) Late Cretaceous Hamsilos volcanic rocks consist of basaltic andesite, trachy-basalt, basaltic trachyandesite and phono-tephrite that display por-

phyric, microlitic porphyric, hyalo-microlitic porphyric, vesicular and glomeroporphyric textures. The rocks include clinopyroxene, plagioclase, biotite, analcime and magnetite/Ti–magnetite.

- (2) On the basis of clinopyroxene thermobarometric calculations, magmas of the shoshonitic rocks crystallised at temperature ranging from 1133 to 1187 °C and at pressure ranging from 1.4 to 6.3 kbar. Whereas, the high-K calc-alkaline rocks were characterised at temperature ranging from 1004 to 1174 °C and at pressure ranging from 1.5 to 3.6 kbar.
- (3) The results of clinopyroxene thermobarometry calculations reveal that the ascending magma ponded at 6–18-km depths from shallow crustal magma chambers for the shoshonitic rocks and at 5–12-km depths from mid-crustal levels for the high-K calc-alkaline rocks.
- (4) The $^{40}\text{Ar}/^{39}\text{Ar}$ dating of the exhibits ages between $72.3 \pm .5$ and $79.0 \pm .3$ Ma (Campaian). The volcanic rocks indicate high-K calc-alkaline and shoshonitic affinities. All samples from the studied volcanic series exhibit similar geochemical features, which are characterised by LILE and LREE enrichment and HFSE depletion with no or slightly negative Eu anomalies, suggesting the subduction-related magmas. Fractional crystallisation with minor contamination by upper crustal materials occurred during the evolution of the volcanic rocks.
- (5) Late Cretaceous Hamsilos volcanic rocks present a narrow I_{Sr} range (78 Ma), and the ϵ_{Nd} (78 Ma) values of high-K calc-alkaline and shoshonitic rocks define an array with .70615 to .70796 and –1.0 to –5.0, respectively. The lead isotopic ratios of high-K calc-alkaline rocks ($^{206}\text{Pb}/^{204}\text{Pb}$) = 18.75, ($^{207}\text{Pb}/^{204}\text{Pb}$) = 15.64 and ($^{208}\text{Pb}/^{204}\text{Pb}$) = 38.79) are similar to those of shoshonitic rocks [$^{206}\text{Pb}/^{204}\text{Pb}$] = 18.74–18.80, ($^{207}\text{Pb}/^{204}\text{Pb}$) = 15.65 and ($^{208}\text{Pb}/^{204}\text{Pb}$) = 38.84–38.88].
- (6) In addition, Sr–Nd isotopic and geochemical data reveal that upper crustal assimilation appears plausible in the generation of Hamsilos volcanic rocks. With these geochemical characteristics, an arc setting can be deduced during the generation of Hamsilos volcanic rocks. As a consequence, it can be concluded that the shoshonitic and high-K calc-alkaline rocks were derived from different degree partial melting of an enriched SCLM material metasomatised by fluids and/or sediments from subduction zone.

Acknowledgements

The author would like to thank Cüneyt Şen for helping in the field and for his thorough, constructive reviews and comments.

I appreciate the help of Frank C. Ramos (New Mexico State University) for isotope analyses and Matthew T. Heizler (New Mexico Tech University) for $^{40}\text{Ar}/^{39}\text{Ar}$ geochronology analyses. The author thanks Osman Parlak and Ş. Can Genç for their accurate and constructive comments to improve the paper. Editorial handling by Erdin Bozkurt is also highly appreciated.

Disclosure statement

No potential conflict of interest was reported by the author.

Funding

This work was supported by the Gümüşhane University [BAP Project no: 13.F5114.02.7]; Karadeniz Technical University [Project#: 2008.112.005.5].

Supplemental data

Supplemental data for this article can be accessed at <http://dx.doi.org/10.1080/09853111.2016.1208526>.

References

- Altherr, R., Topuz, G., Siebel, W., Şen, C., Meyer, H. P., Satır, M., & Lahaye, Y. (2008). Geochemical and Sr-Nd-Pb isotopic characteristics of Paleocene plagioclucitites from the Eastern Pontides (NE Turkey). *Lithos*, 105, 149–161.
- Asan, K., Kurt, H., Francis, D., & Morgan, G. (2014). Petrogenesis of the late Cretaceous K-rich volcanic rocks from the Central Pontide orogenic belt, North Turkey. *Island Arc*, 23, 102–124.
- Aydın, F. (2014). Geochronology, geochemistry, and petrogenesis of the Maçka subvolcanic intrusions: Implications for the Late Cretaceous magmatic and geodynamic evolution of the eastern part of the Sakarya Zone, northeastern Turkey. *International Geology Review*, 56, 1246–1275.
- Aydınçakır, E. (2014). The petrogenesis of Early Eocene non-adakitic volcanism in NE Turkey: Constraints on the geodynamic implications. *Lithos*, 208/209, 361–377.
- Aydınçakır, E., & Şen, C. (2011). Sinop ve çevresindeki Volkanik Kayaçların Petrografisi ve Jeokimyası: İlk Bulgular. 64. *Türkiye Jeoloji Kurultayı Bildiri Özleri*, 25–29 Nisan MTA, Ankara (pp. 161–162 (in Turkish with English abstract)).
- Aygül, M., & Okay, A. I. (2012, April 2–6). Geology of Kastamonu-Tosya Transect, Central Pontides. *65th Geological Congress of Turkey, Abstracts book*, Ankara (pp. 54–55).
- Bacon, C. R., & Hirschmann, M. M. (1988). Mg/Mn partitioning as a test for equilibrium between coexisting Fe-Ti oxides. *American Mineralogist*, 73, 57–61.
- Baier, J., Audétat, A., & Keppler, H. (2008). The origin of the negative niobium tantalum anomaly in subduction zone magmas. *Earth and Planetary Science Letters*, 267, 290–300.
- Barbarin, B. (2005). Mafic magmatic enclaves and mafic rocks associated with some granitoids of the central Sierra Nevada batholith, California: Nature, origin, and relations with the hosts. *Lithos*, 80, 155–177.
- Baş, H. (1986). Petrology and geochemistry of the Sinop volcanics. *Geological Bulletin of Turkey*, 29, 143–56.
- Bektaş, O., & Gedik, I. (1988). A new formation with leucite-bearing shoshonitic volcanism in the Kop area (Everekhanları Formation) and its relationship with the evolution of the eastern Pontide arc, NE, Turkey. *Geological Society of Turkey Bulletin*, 31, 11–19.
- Bektaş, O., Şen, C., Atici, Y., & Köprübaşı, N. (1999). Migration of the Upper Cretaceous subduction-related volcanism towards the back-arc basin of the eastern Pontide magmatic arc (NE Turkey). *Geological Journal*, 34, 95–106.
- Bickle, M. J., & Teagle, D. A. H. (1992). Strontium alteration in the Troodos ophiolite: Implications for fluid fluxes and geochemical transport in mid-ocean ridge hydrothermal systems. *Earth and Planetary Science Letters*, 113, 219–237.
- Boynton, W. V. (1984). Cosmochemistry of the rare earth elements: Meteorite studies. In P. Henderson (Ed.), *Rare earth element geochemistry* (pp. 63–114). Amsterdam: Elsevier.
- Bradshaw, T. K., & Smith, E. I. (1994). Polygenetic quaternary volcanism at Crater Flat, Nevada. *Journal of Volcanology and Geothermal Research*, 63, 165–182.
- Çapan, U. Z. (1984). Ankara melanji içindeki zeolitli alkali bazaltik volkanizmanın karakteri ve yaşı hakkında. *Türkiye Jeoloji Kurumu 38. Bilimsel ve Teknik Kurultayı*, Bildiri özetleri (pp. 121–123) (in Turkish with English abstract).
- Chen, F., Hegner, E., & Todt, W. (2000). Zircon ages and Nd isotopic and chemical compositions of orthogneisses from the Black Forest, Germany: Evidence for a Cambrian magmatic arc. *International Journal of Earth Sciences*, 88, 791–802.
- Chen, W., & Arculus, R. J. (1995). Geochemical and isotopic characteristics of lower crustal xenoliths, San Francisco Volcanic Field, Arizona, USA. *Lithos*, 110, 99–119.
- Conticelli, S., Avanzinelli, R., Marchionni, S., Tommasini, S., & Melluso, L. (2011). Sr-Nd-Pb isotopes from the Radicefani Volcano, Central Italy: Constraints on heterogeneities in a veined mantle responsible for the shift from ultrapotassic shoshonite to basaltic andesite magmas in a post-collisional setting. *Mineralogy and Petrology*, 103, 123–148.
- Dewey, J. F., Pitman, W. C., Ryan, W. B. F., & Bonnin, J. (1973). Plate tectonics and the evolution of the Alpine system. *Geological Society of America Bulletin*, 84, 3137–3180.
- Dokuz, A., Uysal, İ., Siebel, W., Turan, M., Duncan, R., & Akçay, M. (2013). Post-collisional adakitic volcanism in the eastern part of the Sakarya Zone, Turkey: Evidence for slab and crustal melting. *Contributions to Mineralogy and Petrology*, 166, 1443–1468.
- Dungan, M. A., & Rhodes, J. M. (1978). Residual glasses and melt inclusions in basalts from DSDP Legs 45 and 46: Evidence for magma mixing. *Contributions to Mineralogy and Petrology*, 67, 417–431.
- Elliott, T., Plank, T., Zindler, A., White, W., & Bourdon, B. (1997). Element transport from slab to volcanic front at the Mariana arc. *Journal of Geophysical Research: Solid Earth*, 102, 14991–15019.
- Ercan, T., & Gedik, A. (1983). Pontidler'deki volkanizma. *Jeoloji Mühendisliği Derg.*, 18, 3–22.
- Ersoy, E. Y., & Helvacı, C. (2016). Geochemistry and petrology of the lower Miocene bimodal volcanic units in the Tunçbilek–Dömaniç basin, western Anatolia. *International Geology Review*, 58, 1234–1252.
- Eyüboğlu, Y. (2010). Late Cretaceous high-K volcanism in the Eastern Pontide orogenic belt, and its implications for the geodynamic evolution of NE Turkey. *International Geology Review*, 52, 142–186.
- Eyuboglu, Y., Chung, S. L., Santosh, M., Dudas, F. O., & Akaryalı, E. (2011a). Transition from shoshonitic to adakitic magmatism in the eastern Pontides, NE Turkey: Implications for slab window melting. *Gondwana Research*, 19, 413–429.
- Eyuboglu, Y., Santosh, M., Dudas, F. O., Chung, S. L., & Akaryalı, E. (2011b). Migration magmatism in a continental arc: Geodynamics of the Eastern Mediterranean revisited. *Journal of Geodynamics*, 52, 2–15.
- Fitton, J. G., James, D., & Leeman, W. P. (1991). Basic magmatism associated with late Cenozoic extension in the western United States: Compositional variations in space and time. *Journal of Geophysical Research*, 96, 13693–13712.

- Foley, S. F. (1992). Vein-plus-wall-rock melting mechanisms in the lithosphere and the origin of potassic alkaline magmas. *Lithos*, 28, 435–453.
- Foley, S. F., Venturelli, G., Green, D. H., & Toscani, L. (1987). The ultrapotassic rocks: Characteristics, classification, and constraints for petrogenetic models. *Earth Science Reviews*, 24, 81–134.
- Frey, F. A. (1980). The origin of pyroxenites and garnet pyroxenites from salt lake crater, Oahu, Hawaii: Trace element evidence. *American Journal of Science*, 280, 427–449.
- Fujimaki, H., Tatsumoto, M., & Aoki, K. (1984). Partition coefficients of Hf, Zr and REE between phenocrysts and groundmasses. Proceedings of the 4th Lunar Science Conference 2. *Journal of Geophysical Research*, 89, B662–B672.
- Gedik, A., & Korkmaz, S. (1984). Sinop havzasının jeolojisi ve petrol olanakları [Geology and petroleum possibilities of the Sinop basin]. *Journal of Geological Engineering*, 19, 53–79 (in Turkish with English abstract).
- Genç, S. C., Gulmez, F., Karacık, Z., Tuysuz, O., Prelevic, D., Roden, M. F., ... Billor, M. Z. (2014). Subduction-related High-to Ultrahigh-Potassic Rocks of the Ankara-Erzincan Suture Belt of Turkey: A geochemical and isotopic approach to source and petrogenesis. *Geophysical Research Abstracts*, 16, 365 pp., EGU General Assembly.
- Genç, S. C., & Yilmaz, Y. (1995). Evolution of the Triassic continental margin, Northwest Anatolia. *Tectonophysics*, 243, 193–207.
- Gill, J. B. (1981). *Orogenic andesites and plate tectonics*. Berlin: Springer Verlag.
- Goncuoglu, M. C., Turhan, N., & Tekin, K. (2003). Evidence for the Triassic rifting and opening of the Neotethyan İzmir-Ankara Ocean, northern edge of the Tauride-Anatolide Platform, Turkey. *Bulletin of Geological Society of Italy*, 2, 203–212.
- Görür, N., Monod, O., Okay, A.İ., Şengör, A. M. C., Tüysüz, O., Yiğitbaş, E., ... Akkök, R. (1997). Paleogeographic and tectonic position of the Carboniferous rocks of the western Pontides (Turkey) in the frame of the Variscan belt. *Bulletin de la Société géologique de France*, 168, 197–205.
- Green, T. H. (1995). Significance of Nb/Ta as an indicator of geochemical processes in the crust-mantle system. *Chemical Geology*, 120, 347–359.
- Green, D. H., Schmidt, M. W., & Hibberson, W. O. (2004). Island-arc Ankaramites: Primitive melts from fluxed refractory Lherzolitic Mantle. *Journal of Petrology*, 45, 391–403.
- Greene, A. R., Debari, S. M., Kelemen, P. B., Blusztajn, J., & Clift, P. D. A. (2006). Detailed geochemical study of Islan Arc Crust: The Talkeetna Arc section, South-Central Alaska. *Journal of Petrology*, 47, 1051–1093.
- Griffin, W. L., Wang, X., Jackson, S. E., Pearson, N. J., O'Reilly, S. Y., Xu, X. S., & Zhou, X. M. (2002). Zircon chemistry and magma mixing, SE China: In-situ analysis of Hf isotopes, Tonglu and Pingtan igneous complexes. *Lithos*, 61, 237–269.
- Gülmez, F., & Genc, S. C. (2015). Amasya Civarı Geç Kretase Yaşlı Ultrapotasik Volkaniklerinde Farklılaşma Süreçleri [Differentiation Processes in Late Cretaceous Ultrapotassic Volcanics Around Amasya]. *Maden Teknik Arama Dergisi*, 151, 153–172 (in Turkish with English abstract).
- Gupta, A. K., & Fyfe, W. S. (1975). Leucite survival; the alteration to analcime. *The Canadian Mineralogist*, 13, 361–363.
- Halsort, S. P., & Rose, W. I. (1991). Mineralogical relations and magma mixing in calc-alkaline andesites from Lake Atitlan, Guatemala. *Mineralogy and Petrology*, 45, 47–67.
- Hart, S. (1984). A large-scale isotope anomaly in the Southern Hemisphere mantle. *Nature*, 309, 753–757.
- Hastie, A. R., Kerr, A. C., Pearce, J. A., & Mitchell, S. F. (2007). Classification of altered volcanic island arc rocks using immobile trace elements: Development of the Th Co discrimination diagram. *Journal of Petrology*, 48, 2341–2357.
- Hawkesworth, C. J., Turner, S., McDermott, F., Peate, D., & Van Calsteren, P. (1997). U-Th isotopes in arc magmas: Implications for element transfer from the subducted crust. *Science*, 276, 551–555.
- Hibbard, M. J. (1981). The magma mixing origin of mantled feldspars. *Contributions to Mineralogy and Petrology*, 76, 158–170.
- Hochstaedter, A. G., Kepezhinskas, P., Defant, M., Drummond, M., & Koloskov, A. (1996). Insights into the volcanic arc mantle wedge from magnesian lavas from the Kamchatka arc. *Journal of Geophysical Research: Solid Earth*, 101, 697–712.
- Hofmann, A. W. (1997). Chemical differentiation of the Earth: The relationship between mantle, continental crust and oceanic crust. *Earth and Planetary Science Letters*, 90, 297–314.
- Irvine, T. N. & Baragar, W. R. A. (1971). A guide to the chemical classification of common volcanic rocks. *Canadian Journal of Earth Science*, 8, 523–548.
- Irving, A., & Frey, F. A. (1978). Distribution of trace elements between garnet megacrysts and host volcanic liquids of kimberlitic to rhyolitic composition. *Geochimica et Cosmochimica Acta*, 42, 771–787.
- Jacobsen, S. B., & Wasserburg, G. J. (1980). Sm-Nd isotopic evolution of chondrites. *Earth and Planetary Science Letters*, 50, 139–155.
- Karlsson, H. R., & Clayton, R. N. (1991). Analcite phenocrysts in igneous rocks: Primary or secondary. *American Mineralogist*, 76, 189–199.
- Karslı, O., Caran, Ş., Dokuz, A., Çoban, H., Chen, B., & Kandemir, R. (2012). A-type granitoids from the Eastern Pontides, NE Turkey: Records for generation of hybrid A-type rocks in a subduction-related environment. *Tectonophysics*, 530–531, 208–224.
- Karslı, O., Dokuz, A., Uysal, İ., Aydın, F., Chen, B., Kandemir, R., & Wijbrans, J. R. (2010). Relative contributions of crust and mantle to generation of Campanian high-K calc-alkaline I-type granitoids in a subduction setting, with special reference to the Harşit Pluton, Eastern Turkey. *Contributions to Mineralogy and Petrology*, 160, 467–487.
- Karslı, O., Uysal, İ., Dilek, Y., Aydın, F., & Kandemir, R. (2013). Geochemical modelling of early Eocene adakitic magmatism in the Eastern Pontides, NE Anatolia: Continental crust or subducted oceanic slab origin? *International Geology Review*, 55, 2085–2095.
- Karslı, O., Ketenci, M., Uysal, İ., Dokuz, A., Aydın, F., Chen, B., ... Wijbrans, J. (2011). Adakite-like granitoid porphyries in the Eastern Pontides, NE Turkey: Potential parental melts and geodynamic implications. *Lithos*, 127, 354–372.
- Kasapoğlu, B., Ersoy, Y. E., Uysal, İ., Palmer, M. R., Zack, T., Koralay, E. O., & Karlsson, A. (2016). The petrology of Paleogene volcanism in the Central Sakarya, Nallıhan Region: Implications for the initiation and evolution of post-collisional, slab break-off-related magmatic activity. *Lithos*, 246–247, 81–98.
- Kaygusuz, A., & Aydınçakır, E. (2009). Mineralogy, whole-rock and Sr–Nd isotope geochemistry of mafic microgranular enclaves in Cretaceous Dagbasi granitoids, Eastern Pontides, NE Turkey: Evidence of magma mixing, mingling and chemical equilibration. *Chemie der Erde-Geochemistry*, 69, 247–277.
- Kaygusuz, A., & Aydınçakır, E. (2011). Petrogenesis of a Late Cretaceous composite pluton from the eastern Pontides: The Dağbaşı pluton, NE Turkey. *Neues Jahrbuch Für Mineralogie*, 188, 211–233.

- Kirchenbaur, M., Munker, C., Schuth, S., Garbe-Schonberg, D., & Marchev, P. (2012). Tectonomagmatic constraints on the sources of Eastern Mediterranean K-rich Lavas. *Journal of Petrology*, 53, 27–65.
- Kuiper, K. F., Deino, A., Hilgen, F. J., Krijgsman, W., Renne, P. R., & Wijbrans, J. R. (2008). Synchronizing rock clocks of earth history. *Science*, 320, 500–504.
- Langmuir, C. H., Vocke, R. D., Hanson, G. N., & Hart, S. R. (1978). A general mixing equation with applications to Icelandic basalts. *Earth and Planetary Science Letters*, 37, 380–392.
- Le Bas, M. J., Le Maitre, R. W., Streckeisen, A., & Zanettin, B. (1986). A chemical classification of volcanic rocks on the total alkali-silica diagram. *Journal of Petrology*, 27, 745–750.
- Le Roex, A. P. (1987). Source regions of mid-ocean ridge basalts; evidence for enrichment processes. In A. M. Menzies & C. J. Hawkesworth (Eds.), *Mantle metasomatism* (pp. 389–422). London: Academic Press.
- Liew, T. C., & Hofmann, A. W. (1988). Precambrian crustal components, plutonic associations, plate environment of the Hercynian Fold Belt of central Europe: Indications from a Nd and Sr isotopic study. *Contributions to Mineralogy and Petrology*, 98, 129–138.
- Luhr, J. F., & Carmichael, I. S. E. (1980). The Colima volcanic complex, Mexico. *Contributions to Mineralogy and Petrology*, 71, 343–372.
- Luhr, J. F., Carmichael, I. S. E., & Varekamp, J. C. (1984). The 1982 eruptions of El Chichón Volcano, Chiapas, Mexico: Mineralogy and petrology of the anhydritebearing pumices. *Journal of Volcanology and Geothermal Research*, 23, 69–108.
- Luhr, J. F., & Kyser, T. K. (1989). Primary igneous analcime: The Colima minettes. *American Mineralogist*, 74, 216–223.
- Macdonald, R., Hawkesworth, C. J., & Heath, E. (2000). The Lesser Antilles volcanic chain: A study in arc magmatism. *Earth Science Reviews*, 49, 1–76.
- Mahoney, J. J., Frei, R., Tejada, M. L. G., Mo, X. X., Leat, P. T., & NaGler, T. P. (1998). Tracing the Indian Ocean mantle domain through time: Isotopic results from old west Indian, east Tethyan, and South Pacific Seafloor. *Journal of Petrology*, 39, 1285–1306.
- Maria, A., & Luhr, J. (2008). Lamprophyres, basanites, and basalts of the western Mexican volcanic belt: Volatile contents and a vein-wallrock melting relationship. *Journal of Petrology*, 49, 2123–2156.
- McDonough, W. F. (1990). Constraints on the composition of the continental lithospheric mantle. *Earth and Planetary Science Letters*, 101, 1–18.
- McKenzie, D. P., & O'Nions, R. X. (1991). Partial melt distributions from inversion of rare earth element concentrations. *Journal of Petrology*, 32, 1021–1091.
- Menzies, M., & Kyle, P. R. (1990). Continental volcanism: A crust-mantle probe. In M. A. Menzies (Ed.), *Continental mantle* (pp. 157–177). Oxford: Clarendon Press.
- Min, K., Mundil, R., Renne, P. R., & Ludwig, K. R. (2000). A test for systematic errors in $^{40}\text{Ar}/^{39}\text{Ar}$ geochronology through comparison with U-Pb analysis of a 1.1 Ga rhyolite. *Geochimica et Cosmochimica Acta*, 64, 73–98.
- Moradian, A. (2008). A contribution to the genesis of analcite after leucite in potassic volcanic rocks of the Nadik area, Kerman, Iran. *Journal of Sciences Islamic Republic of Iran*, 19, 31–48.
- Morimoto, N. (1988). Nomenclature of pyroxenes. *Mineralogical Magazine*, 52, 535–550.
- Münker, C., Wörner, G., Yogodzinski, G., & Churikova, T. (2004). Behaviour of high field strength elements in subduction zones: Constraints from Kamchatka-Aleutian arc lavas. *Earth and Planetary Science Letters*, 224, 275–293.
- Nelson, S. T., & Montana, A. (1992). Sieve-textured plagioclase in volcanic rocks produced by rapid decompression. *American Mineralogist*, 77, 1242–1249.
- Nesbitt, H. W., & Young, G. M. (1982). Early Proterozoic climates and plate motions inferred from major element chemistry of lutites. *Nature*, 299, 715–717.
- Nielsen, C. H., & Sigurdsson, H. (1981). Quantitative methods for electron microprobe analysis of sodium in natural and synthetic glasses. *American Mineralogist*, 66, 547–552.
- Nimis, P. (1995). A clinopyroxene geobarometer for basaltic systems based on crystal-structure modeling. *Contributions to Mineralogy and Petrology*, 121, 115–125.
- Nimis, P., & Taylor, W. R. (2000). Single clinopyroxene thermobarometry for garnet peridotites. Part I. Calibration and testing of a Cr-in-Cpx barometer and an enstatite-in-Cpx thermometer. *Contributions to Mineralogy and Petrology*, 139, 541–554.
- Nimis, P., & Ulmer, P. (1998). Clinopyroxene geobarometry of magmatic rocks Part 1: An expanded structural geobarometer for anhydrous and hydrous, basic and ultrabasic systems. *Contributions to Mineralogy and Petrology*, 133, 122–135.
- Ohta, T., & Arai, H. (2007). Statistical empirical index of chemical weathering in igneous rocks: A new tool for evaluating the degree of weathering. *Chemical Geology*, 240, 280–297.
- Okay, A. I. (2011, April). Metamorphic evolution of the pre-jurassic basement of the Sakarya Zone. *64th Geological Congress of Turkey*, Ankara.
- Okay, A. I., & Şahintürk, O. (1997). Geology of the eastern pontides. In A.G. Robinson (Ed.), *Regional and petroleum geology of the Black Sea and surrounding region* (Vol. 68, pp. 291–311). American Association of Petroleum Geologists Memoir.
- Okay, A. I., Şahintürk, Ö., & Yakar, H. (1997). Stratigraphy and tectonics of the Pulur (Bayburt) region in the Eastern Pontides. *Bulletin of the Mineral Research and Exploration Institute of Turkey*, 119, 1–24.
- Okay, A. I., & Tüysüz, O. (1999). Tethyan sutures of northern Turkey. In B. Durand, L. Jolivet, F. Horvath, & M. Seranne (Eds.), *The Mediterranean basins: Tertiary extension within the Alpine Orogen* (Vol. 156, pp. 475–515). London: Geological Society, Special Publication.
- Okay, A. I., Tuysuz, O., Satir, M., Ozkan-Altiner, S., Altiner, D., Sherlock, S., & Eren, R. H. (2006). Cretaceous and Triassic subduction-accretion, high-pressure-low-temperature metamorphism, and continental growth in the Central Pontides, Turkey. *Geological Society of America Bulletin*, 118, 1247–1269.
- Parker, A. (1970). An index of weathering for silicate rocks. *Geological Magazine*, 107, 501–504.
- Pearce, J. A. (1983). Role of the sub-continental lithosphere in magma genesis at active continental margins. In C. J. Hawkesworth & M. J. Norry (Eds.), *Continental basalts and mantle xenoliths* (pp. 230–249). Cheshire: Shiva.
- Pearce, T. H. (1993). Analcime phenocrysts in igneous rocks; primary or secondary? Discussion. *American Mineralogist*, 78, 225–229.
- Pearce, J. A., Bender, J. F., De Long, S. E., Kidd, W. S. F., Low, P. J., Güner, Y., ... Mitchell, J. J. (1990). Genesis of collision volcanism in Eastern Anatolia, Turkey. *Journal of Volcanology and Geothermal Research*, 44, 189–229.
- Plank, T., & Langmuir, C. H. (1998). The chemical composition of subducting sediment and its consequences for the crust and mantle. *Chemical Geology*, 145, 325–394.
- Putirka, K. D. (2008). Thermometers and barometers for volcanic systems. In K. D. Putirka & F. Tepley (Eds.), *Reviews in mineralogy and geochemistry* (Vol. 69, pp. 61–120). Washington: Mineralogical Society of America.

- Putirka, K. D., Johnson, M., Kinzler, R., & Longhi, J. (1996). Thermobarometry of mafic igneous rocks based on clinopyroxene-liquid equilibria, 0–30 kbar. *Contributions to Mineralogy and Petrology*, 123, 92–108.
- Putirka, K. D., Mikaelian, H., & Ryerson, F. (2003). New clinopyroxene-liquid thermobarometers for mafic, evolved, and volatile-bearing lava compositions, with applications to lavas from Tibet and the Snake River Plain, Idaho. *American Mineralogist*, 88, 1542–1554.
- Putnis, A., Putnis, C., & Giampaolo, C. (1994). The microtexture of analcime phenocrysts in igneous rocks. *European Journal of Mineralogy*, 6, 627–632.
- Ramos, F.C. (1992). *Isotope Geology of Metamorphic Core of the Central Grouse Creek Mountains, Box Elder Country, Utah* (MSc thesis), University of California, Los Angeles.
- Rollinson, H. R. (1993). *Using geochemical data: Evolution, presentation, interpretation* (pp. 352). New York, NY: Wiley.
- Şengör, A. M. C., Özeren, S., Genç, T., & Zor, E. (2003). East Anatolian high plateau as a mantle-supported, North-south shortened domal structure. *Geophysical Research Letters*, 30(24), 8045. doi:10.1029/2003gl017858
- Şengör, A. M. C., & Yilmaz, Y. (1981). Tethyan evolution of Turkey: A plate tectonic approach. *Tectonophysics*, 75, 181–241.
- Shaw, D. M. (1970). Trace element fractionation during anatexis. *Geochimica et Cosmochimica Acta*, 34, 237–243.
- Simonetti, A., Shore, M., & Bell, K. (1996). Diopside phenocrysts from nephelinite lavas, Napak Volcano, Eastern Uganda: Evidence for magma mixing. *Canadian Mineralogist*, 34, 411–442.
- Sisson, T. W., Ratajeski, K., Hankins, W. B., & Glazner, A. F. (2005). Voluminous granitic magmas from common basaltic sources. *Contributions to Mineralogy and Petrology*, 148, 635–661.
- Smith, T. E., Holm, P. E., & Thirlwall, M. F. (2008). The geochemistry of the volcanic rocks of Canouan, Grenadine islands, Lesser Antilles arc. *Geological Journal*, 43, 582–604.
- Smith, E. I., Sánchez, A., Walker, J. D., & Wang, K. (1999). Geochemistry of mafic magmas in the Hurricane Volcanic field, Utah: Implications for small- and large-scale chemical variability of the lithospheric mantle. *The Journal of Geology*, 107, 433–448.
- Speer, J. A. (1984). Micas in igneous rocks. In S. W. Bailey (Ed.), *Micas: Reviews in mineralogy and geochemistry* (Vol. 13, pp. 299–356). Washington, DC: Mineralogical Society of America.
- Staudigel, H., Davies, G. R., Hart, S. R., Marchant, K. M., & Smith, B. M. (1995). Large scale isotopic Sr, Nd and O isotopic anatomy of altered oceanic crust: DSDP/ODP sites 417/418. *Earth and Planetary Science Letters*, 130, 169–185.
- Stimac, J. A., & Pearce, T. H. (1992). Textural evidence of mafic-felsic magma interaction in dacite lavas, Clear Lake, California. *American Mineralogist*, 77, 795–809.
- Streck, M. J. (2008). Mineral textures and zoning as evidence for open system processes. In K. D. Putirka & F. J. Tepley III (Eds.), *Minerals, inclusions and volcanic processes. Reviews in Mineralogy and Geochemistry* (pp. 595–622). Washington, DC: Mineralogical Society of America and Geochemical Society.
- Sun, S., & McDonough, W. F. (1989). Chemical and isotopic systematics of oceanic basalt: Implications for mantle composition and processes. In A. D. Saunders & M. J. Norry (Eds.), *Magmatism in the ocean basins* (Vol. 42, pp. 313–345). London: Geological Society of London Special Publication.
- Tatsumi, Y., Hamilton, D. L., & Nesbitt, R. W. (1986). Chemical characteristics of fluid phase released from a subducted lithosphere and origin of arc magmas: Evidence from high-pressure experiments and natural rocks. *Journal of Volcanology and Geothermal Research*, 29, 293–309.
- Taylor, S. R., & McLennan, S. M. (1985). *The continental crust. Its composition and evolution* (pp. 312). Oxford: Blackwell.
- Tekeli, O. (1981). Subduction complex of pre-Jurassic age, northern Anatolia, Turkey. *Geology*, 9, 68–72.
- Tepley, F. J., Davidson, J. P., Tilling, R. L., & Arth, J. G. (2000). Magma mixing, recharge and eruption histories recorded in plagioclase phenocrysts from El Chichón Volcano, Mexico. *Contributions to Mineralogy and Petrology*, 41, 1397–1411.
- Thirlwall, M. F., Smith, T. E., Graham, A. M., Theodorou, N., Hollings, P., Davidson, J. P., & Arculus, R. J. (1994). High field strength element anomalies in arc lavas: Source or process? *Journal of Petrology*, 35, 819–838.
- Tokel, S. (1983). Doğu Pontidler'in Mesozoyik ve Tersiyerdeki gelişimleri, bu gelişmelerin Kuzey Anadolu sismik zonuile muhtemel ilgileri. *Cumhuriyetin 50. Yılı Yerbilimleri Kongresi Tebliğler kitabı* (pp. 1–4). Ankara.
- Topuz, G., Altherr, R., Schwarz, W. H., Siebel, W., Satır, M., & Dokuz, A. (2005). Post-collisional plutonism with adakite-like signatures: The Eocene Saraycık granodiorite (Eastern Pontides, Turkey). *Contributions to Mineralogy and Petrology*, 150, 441–455.
- Tribuzio, R., Thirlwall, M. F., Vannucci, R., & Matthew, F. (2004). Origin of the Gabbro-Peridotite Association from the Northern Apennine Ophiolites (Italy). *Journal of Petrology*, 45, 1109–1124.
- Tsuehaya, A. (1985). Dissolution kinetics of plagioclase in the melt of the system diopside-albite-anorthite, and origin of dusty plagioclase in andesites. *Contributions to Mineralogy and Petrology*, 89, 1–16.
- Turner, S., Hawkesworth, C., Rogers, N., Bartlett, J., Worthington, T., Hergt, J., ... Smith, I. (1997). ^{238}U - ^{230}Th disequilibrium, magma petrogenesis and flux rates beneath the depleted Tonga-Kermadec island arc. *Geochimica et Cosmochimica Acta*, 61, 4855–4884.
- Tüysüz, O. (1990). Tectonic evolution of a part of the Tethyside orogenic collage: The Kargi Massif, northern Turkey. *Tectonics*, 9, 141–160.
- Tüysüz, O. (1999). Geology of the Cretaceous sedimentary basins of the Western Pontides. *Geological Journal*, 34, 75–93.
- Uchida, E., Endo, S., & Makino, M. (2007). Relationship between solidification depth of granitic rocks and formation of hydrothermal ore deposits. *Resource Geology*, 57, 47–56.
- Ustaömer, T., & Robertson, A. H. F. (1993). A Late Palaeozoic-Early Mesozoic marginal basin along the active southern continental margin of Eurasia: Evidence from the central Pontides (Turkey) and adjacent regions. *Geological Journal*, 28, 219–238.
- Ustaömer, T., & Robertson, A. H. F. (2010). Late Palaeozoic-Early Cenozoic tectonic development of the Eastern Pontides (Artvin area), Turkey: Stages of closure of Tethys along the southern margin of Eurasia. *Geological Society, London, Special Publications*, 340, 281–327.
- Varol, E. (2013). The derivation of potassic and ultrapotassic alkaline volcanic rocks from an orogenic lithospheric mantle source: The case of the Kalecik district, Ankara, Central Anatolia, Turkey. *Journal of Mineralogy and Geochemistry*, 191, 55–73.
- Weaver, B. L., Wood, D. A., Tarney, J., & Joron, J. (1987). Geochemistry of ocean island basalt from the South Atlantic: Ascension, Bouvet, St. Helena, Gough and Tristan da Cunda. In J. G. Fitton & B. G. J. Upton (Eds.), *Alkaline igneous rocks* (Vol. 30, pp. 253–267). London: Geological Society, Special Publications.
- Wilson, M. (1989). *Igneous petrogenesis* (pp. 466). Oxford: Oxford University Press.

- Wones, D. R., & Eugster, H. P. (1965). Stability of biotite: Experiment, theory, and application. *American Mineralogist*, 50, 1228–1272.
- Woodhead, J. D., Hergt, J. M., Davidson, J. P., & Eggins, S. M. (1991). Hafnium isotope evidence for conservative element mobility during subduction zone processes. *Earth and Planetary Science Letters*, 102, 331–346.
- Xu, J. F., & Castillo, P. R. (2004). Geochemical and Nd–Pb isotopic characteristics of the Tethyan asthenosphere: Implications for the origin of the Indian Ocean mantle domain. *Tectonophysics*, 393, 9–27.
- Xu, J. F., Castillo, P. R., Chen, F. R., Niu, H. C., Yu, X. Y., & Zhen, Z. P. (2003). Geochemistry of late Paleozoic mafic igneous rocks from the Kuerti area, Xinjiang, northwest China: Implications for backarc mantle evolution. *Chemical Geology*, 193, 137–154.
- Yılmaz, Y., & Şengör, A. M. C. (1985). Paleotethyan ophiolites in northern Turkey: Petrology and tectonic setting. *Ofioliti*, 10, 485–504.
- Yılmaz, Y., Tüysüz, O., Yiğitbaş, E., Genç, Ş. C., & Şengör, A. M. C. (1997). Geology and tectonic evolution of the Pontides. In A. G. Robinson (Ed.), *Regional and petroleum geology of the Black Sea and surrounding region* (Vol. 68, pp. 183–226). American Association of Petroleum Geologists Memoir.
- Yücel, C., Arslan, M., Temizel, İ., & Abdioğlu, E. (2014b). Volcanic facies and mineral chemistry of Tertiary volcanics in the northern part of the Eastern Pontides, northeast Turkey: Implications for pre-eruptive crystallization conditions and magma chamber processes. *Mineralogy and Petrology*, 108, 439–467.
- Yücel, C., Temizel, İ., Abdioğlu, E., Arslan, M., & Yağcıoğlu, U. C. (2014a). Origin of analcimes in the Tertiary volcanic rocks from the Eastern Pontides (NE Turkey): A textural, mineralogical and geochemical approach. *Neues Jahrbuch Für Mineralogie*, 191, 277–299.
- Zindler, A., & Hart, S. R. (1986). Chemical geodynamics. *Annual Review of Earth and Planetary Sciences*, 14, 493–571.